CHALMERS


# Corrosion Mechanisms under Organic Coatings

## A study in relation to Next Generation´s Pretreatments

**Master of Science Thesis in the International Master´s program Chemical Engineering**

**JOHANNA KARLSSON**

Department of Chemical and Biological Engineering
*Division of Environmental Inorganic Chemistry*
*Corrosion Science*
CHALMERS UNIVERSITY OF TECHNOLOGY
Göteborg, Sweden, 2011

MASTER'S THESIS

# Corrosion Mechanisms under Organic Coatings

## A study in relation to Next Generation's Pretreatments

*Master´s Thesis in the International Master´s program Chemical Engineering*

**JOHANNA KARLSSON**

Department of Chemical and Biological Engineering
Division of Environmental Inorganic Chemistry
Corrosion Science
CHALMERS UNIVERSITY OF TECHNOLOGY
Göteborg, Sweden, 2011

Corrosion Mechanisms under Organic Coatings
A study in relation to Next Generation's Pretreatments
*Master´s Thesis in the International Master´s program Chemical Engineering*
**JOHANNA KARLSSON**



Master's Thesis
Department of Chemical and Biological Engineering
Division of Environmental Inorganic Chemistry
Corrosion Science
Chalmers University of Technology
SE-412 96 Göteborg
Sweden
Telephone: + 46 (0)31-772 1000

Göteborg, Sweden, 2011

**Corrosion Mechanisms under Organic Coatings**

A study in relation to Next Generation's Pretretments

Master's Thesis in the International Master's program Chemical Engineering
JOHANNA KARLSSON
Department of Chemical and Biological Engineering
Division of Environmental Inorganic Chemistry
Corrosion Science
Chalmers University of Technology
Göteborg, Sweden, 2011

## SUMMARY

The demands on the corrosion protection in the automotive industry are very extensive. A car is subjected to various environments and there are many factors affecting the corrosion. There are thus high demands also on the corrosion testing. Many studies have been made concerning atmospheric corrosion but corrosion under a paint coating system is fairly unexplored. Such studies are important in understanding the corrosion mechanism possible in automotive corrosion. Phosphating is the pretreatment used in the automotive industry today and offer an excellent corrosion protection to the painted metal. However due to environmental aspects and possible legislation a need for new pretreatments, next generation pretreatments (NGPT) have developed and are under evaluation. Two types of NGPT´s are of greatest interest, a silane based one and a zirconium based one.

The purpose of this project is to investigate corrosion under organic coating in an attempt to understand the corrosion mechanisms. The influence of different pretreatments in this context is also studied.

The most existent corrosion product found was a zinc hydroxy chloride called simonkolleite [$Zn_5Cl_2(OH)_8*H_2O$] despite different pretreatments and exposure methods. This compound was found in a growth ring pattern on all materials from the cyclic corrosion test. The growth rings are related to the cycles in corrosion test chambers. The growth ring pattern is more distinct on the NGPT panels. The corrosion is spread in a circular manner from a small cathodic spot in the scribe. The scribe is applied to act as an initiation point for the corrosion. The analyses were preformed mainly with SEM/EDS and to some extent with optical microscopy and FTIR.

The study shows a clear difference in morphology between the different pretreatments, however bending test shows no differences in adhesiveness to paint coating. The bending test showed that the fracture occurred within the pretreatment layer. In the cyclic corrosion test, however, the pretreatment layer is present on the paint side of the fracture.

Key words: corrosion mechanisms, pretreatment, silane, zirconium, corrosion protection, automotive coating.

**Korrosionsmekanismer under lack**
Ett arbete i samband med Nästa Generations Förbehandlingar

Examensarbete inom Civilingenjörsprogrammet Kemiteknik
JOHANNA KARLSSON
Institutionen för kemi- och bioteknik
Avdelningen för oorganisk miljökemi
Korrosion
Chalmers tekniska högskola
Göteborg, Sverige, 2011

## SAMMANFATTNING

Det ställs höga krav på korrosionsskydd inom bilindustrin. En bil utsätts för olika miljöer under en livstid där det kan finnas många faktorer som påverkar korrosionen. Därför ställs det också höga krav på korrosionstester. Många tidigare studier behandlar atmosfärisk korrosion men få behandlar korrosion under lack. Detta är ett viktigt område för förståelsen kring korrosion inom bilindustrin. Fosfatering är den mest förekommande förbehandlingsmetoden som används idag och bidrar med utmärkt korrosionsskydd till den lackerade metallen. Nya förbehandlingsmetoder (NGPT, nästa generations förbehandlingar) är dock under utveckling på grund av miljöaspekter samt möjlig lagstiftning rörande fosfateringsprocessen. Främst två förbehandlingar är av största intresse, en silanbaserad och en zirkoniumbaserad.

Syftet med arbetet var att undersöka korrosion under lack i ett försök att förstå de korrosionsmekanismer som är verksamma. Undersökningen genomfördes i samband med olika förbehandlingsmetoder.

Den mest förekommande korrosionsprodukten som identifierades var en zinkhydroxyklorid, simonkolleit [$Zn_5Cl_2(OH)_8*H_2O$] gällande för material med olika förbehandlingsmetoder samt exponering. Denna förening var uppbyggd i ett årsringsmönster och hittades på alla material från den cykliska exponeringen. Årsringsmönstret var tydligast uttalat på panelerna med NGPT. Årsringarna är relaterade till de olika cyklerna i korrosionskammaren. Korrosionen har en cirkelformad utbredning och sprids från en liten punkt i ritsen. Ritsen fungerar som initieringsområde för korrosionen. Analyserna utfördes mestadels med SEM/EDS men även till viss del med FTIR.

Studien visade en klar skillnad i morfologi mellan de olika förbehandlingsskikten, men resultat från böjprov påvisade ingen skillnad i vidhäftning till ovanliggande lackskikt. Böjprovet visade att brottet gick i förbehandlingsskiktet. Alla förbehandlingar visar god vidhäftning till närliggande ytor och är fortfarande intakta efter exponering. De intakta förbehandlingsskikten sitter på lacksidan.

Nyckelord: korrosionsmekanismer, förbehandling, silaner, zirkonium, korrosionsskydd, billack.

# Contents

## Preface

In this master thesis, an investigation to understand the corrosion mechanisms occurring beneath a coating system in relation to next generation's pretreatments was performed. The project was introduced due to possible legislation affecting the currently used pretreatment process in the automotive industry. The work has been performed at Volvo Car Corporation in Torslanda under the supervision of Håkan Mattsson (Ph.D.). I would like to express my sincere regards to Håkan Mattsson for invaluable support throughout the whole project and tremendous commitment to my work. I want to acknowledge Anders Makkonen, unit manager, for giving me the opportunity to carry out the project and to everyone at the surface treatment centre for making my time enjoyable. The project was initiated in January 2011 and completed in June 2011.

I also would like to express my sincere regards to Ass. Professor Jan-Erik Svensson and examiner Professor Lars-Gunnar Johansson at Chalmers University of Technology for their guidance and support. Finally I would like to express my appreciation to my opponent Magnus Bergh for continuous assistance.

Göteborg, June 2011

Johanna Karlsson

# 1 Introduction

## 1.1 Background

Corrosion protection in the car industry is of great importance and the demands on the business within this field are large. A vehicle is subjected to various environments during a lifetime and there are many factors that affect corrosion, e.g. humidity, temperature, a variety of air pollutants such as Cl, $SO_x$ and $NO_x$ and by winter road, de-icing salts. In marine areas and coastal cities the environment is particularly aggressive and highly subjected to corrosion [1,2]. The demands are not only high for the product itself but also for the corrosion testing used to evaluate the corrosion resistance of different metals. The accelerated corrosion tests are developed mainly empirically with some physical mechanisms taken under consideration. The key is to measure corrosion in a laboratory scale and to get corrosion behaviour closely related to field exposure but at the same time have a high acceleration factor [2].

Overall knowledge of corrosion mechanisms under an organic coating is lacking and is a prerequisite in understanding the accelerated corrosion tests better. Most studies focus on unprotected substrates; the mechanisms and theories are thus different if the substrate is coated. In this work a literature survey has been done in order to serve as a state of the art basis for the present investigation in order to get complete understanding of corrosion under paint coating.

The most common pretreatment process within the automotive industry today is phosphating which offers an excellent corrosion protection to the painted metal. However due to environmental aspects and possible legislation a need for new pretreatments, next generation pretreatments (NGPT) have developed and are under evaluation. When talking about NGPT´s two types are of interest; a silane based one and a zirconium based one. The layer formed from the NGPT´s present on the market is a lot thinner than the traditional phosphating layer. Knowledge of corrosion mechanisms will help understanding the corrosion methods better in an attempt to understand how well suited the methods are with the NGPT´s.

## 1.2 Objective

The overall goal is to evaluate/ modify the corrosion tests used today to make sure that they are reliable and highly accelerated based on the knowledge of corrosion mechanisms under paint with different pretreatment processes. This study will contribute with important information regarding corrosion mechanisms active correlated to the NGPT´s as well as for the currently used phosphating. The aim with the technical reference is to emphasize the theories existing today followed by investigations regarding these theories.

## 1.3 Method

The study will begin with a thorough literature review of the existing material in the area present today and will be put together as a technical reference. A number of corrosion samples are available which were produced in relation to a primary evaluation of the NGPT´s. The panels are coated and scribed to initiate corrosion and placed in climate chambers aimed to simulate natural conditions at accelerated speed. The pretreatment is either silane- or zirconium based or the traditional phosphating. Panels from one year of field exposure are also available.

The experimental part of the thesis will include characterization of corrosion products of different samples and of the different pretreatments. The characterization and analysis will

primarily be performed using optical microscopy, SEM and EDS but to some extent also FTIR.

## 1.4 Limitations

Due to the limited time available for this master thesis some limitations need to be set. A first restriction is to focus on hot dipped galvanized steel, HDG. A large amount of the material on the vehicle is made out of HDG and this is therefore an important material. Phosphating is what is used today in the automotive industry and is of great importance. In order to get thorough knowledge on the corrosion mechanisms active underneath paint coating a lot of focus will be on analyzing phosphated substrates before moving on to the substrates with the NGPT´s.

# 2 Technical Reference

## 2.1 Introduction

The technical reference is based on a literature survey performed during January-April 2011 with search words e.g. corrosion mechanisms, pretreatment, silane, zirconium, corrosion protection and automotive coating. The purpose is to get thorough information regarding the work done before in areas including NGPT's and corrosion mechanisms under organic coating. The focus on the technical reference is attended to corrosion under organic coating on hot-dip galvanized steel.

## 2.2 The Automotive Body Panel

A general model of an automotive coating system is a substrate on which different layers are applied (Fig. 2.1). Each layer has its own function and the whole system protects the substrate in three types of coatings; metallic, inorganic and organic [3].

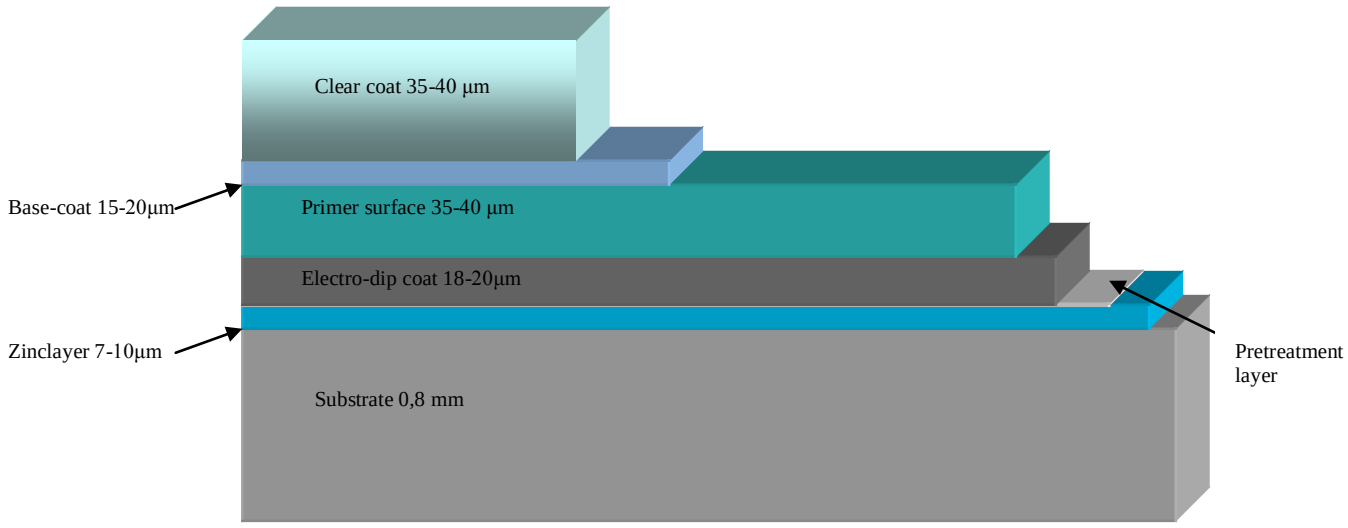


Figure 2.1. *Complete automotive coating system* [4].

### 2.2.1 Metallic Coating

There are a number of zinc-coated steel sheet varieties of which hot-dip galvanized steel (HDG) is the most commonly used in the automotive industry. HDG is produced by immersing steel in molten zinc or zinc alloy forming a zinc layer with a thickness of roughly

7-30μm [5]. On the outer car body skin the HDG zinc thickness is usually 7 μm. The zinc coating provides the substrate with a resistance to corrosion by cathodic control.

### 2.2.2 Pretreatments

Previous studies have shown the importance of pretreatments and their beneficial effect on corrosion protection [3, 6]. In the pretreatment process the product is prepared for the paint application and should make for a better adhesion to the paint and for a better finish of the painted sheet. The pretreatment is also intended to offer corrosion protection in form of a chemical or electrical barrier. The pretreatment process is a multistep process starting with a degreasing step with the purpose to make sure the substrate is free from contaminants. All pretreatments have an initial degreasing step with the main function to remove soil, soot, oil and possible oxides formed on the metal substrate. The degreasing etches off a tenth of a micrometer of the surface at a high pH which makes the metal surface highly reactive. The metal reacts with surrounding water forming a hydroxide layer, which is of great importance for the NGPT´s, especially for the silane based one [7].

#### 2.2.2.1 Phosphate Coating

The phosphating process is since many decades state of the art for treating the body prior to painting in the automotive industry. It is an essential metal surface treatment process and acts as a foundation for paint to obtain firm adhesion and offer corrosion protection. There are different types of zinc phosphating baths; monocation (Zn), bication (Zn/Mn) and trication (Zn/Ni/Mn). This field has been investigated by Ogle. Trication is the most commonly used variant in the automotive industry. The treatment takes place in a mixed spray-dip process and involves dissolution of the topmost surface layer. The substrate is put in a phosphoric acid solution containing metal ions e.g. zinc, manganese and nickel. An accelerator, e.g. nitrate, is added to the reaction which is reduced at the cathode. The other reactions occurring are oxidation of the metal at the anode and hydrogen reduction at the cathode together with the nitrate reduction [6].

The total reaction results in an increase in pH at the substrate surface and the metal ions precipitate as insoluble phosphate crystals (Fig. 2.2). The metal is oxidized at the anode and at the cathode hydrogen is reduced. The formation of hydrogen gas at the cathode results in a pH increase leading to phosphate crystal precipitation. A phosphate crystal layer is obtained with a coating weight of 2-5 g/m$^2$ and a crystal size of 2-15 μm (Fig. 2.3). The crystalline coating should cover almost the entire metal surface (~99%) and be evenly distributed over the surface which is important since the phosphate crystals are poor conductors and thus the reactions take place on the uncovered surface. Different crystals are formed depending on the substrate and the most common ones are phosphophyllite and hopeite. The coating formation is initiated on nucleation sites on the substrate. The nucleation sites usually consist of titanium colloids [8].

| | | |
|---|---|---|
| Steel: | $FeZn_2(PO_4)_2 * 4H_2O(s)$ | *phosphophyllite* |
| Zinc (HDG): | $Zn_3(PO_4)_2 * 4H_2O(s)$ | *hopeit* |

Hopeit is also formed on aluminum and the crystals are characteristically rather large (approximately 10 μm) and have a little less coverage across the surface [7].

*Precipitation or formation of coating:*

$$3Zn^{2+} + 2PO_4^{3-} \rightarrow Zn_3PO_4 * 4H_2O(s) \qquad (2.1)$$

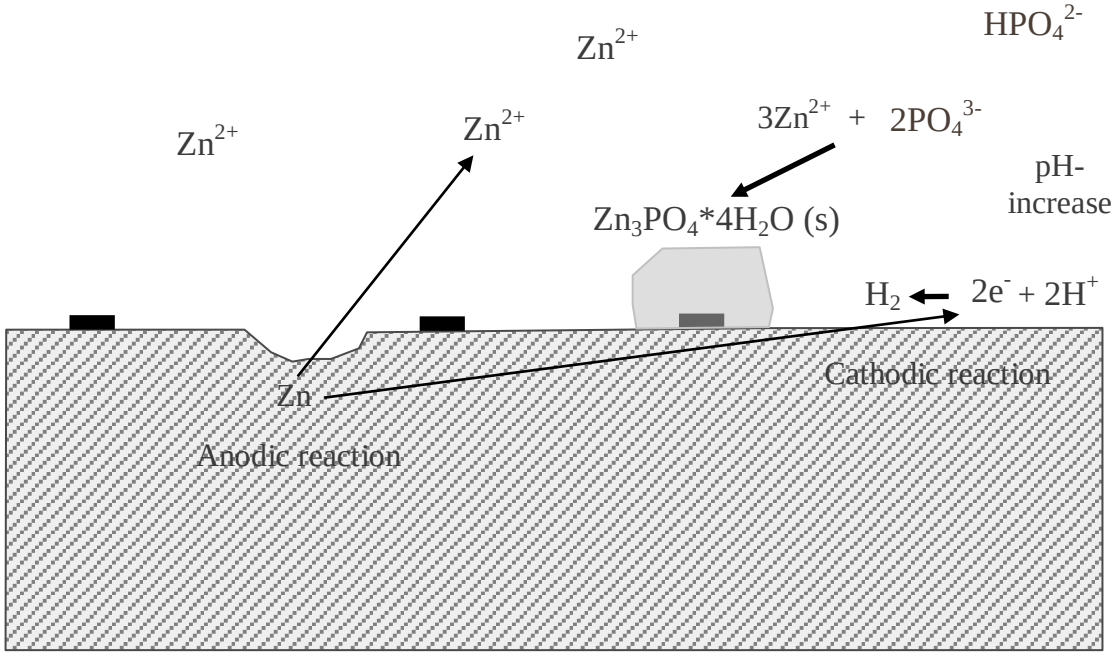


Figure 2.2. *General figure over the phosphate formation. The blue rectangular figures are nucleation sites* [7].

The good adhesion is obtained since paint flows down into the pores of the crystalline phosphate coating creating a key and lock effect. The phosphate layer has an electrical isolating effect which prohibits the coupled anodic- and cathodic reactions and therefore decreases the corrosion rate [9,10]. A study made by Ogle shows that using a Zn/Ni/Mn ion composition in phosphating bath provides alkaline resistance, which affects the corrosion in a favourable way. The corrosion resistance is increased due to buffer effect. Ogle also shows that some types of phosphating get more stable by adding e.g. Mn to the process [6].

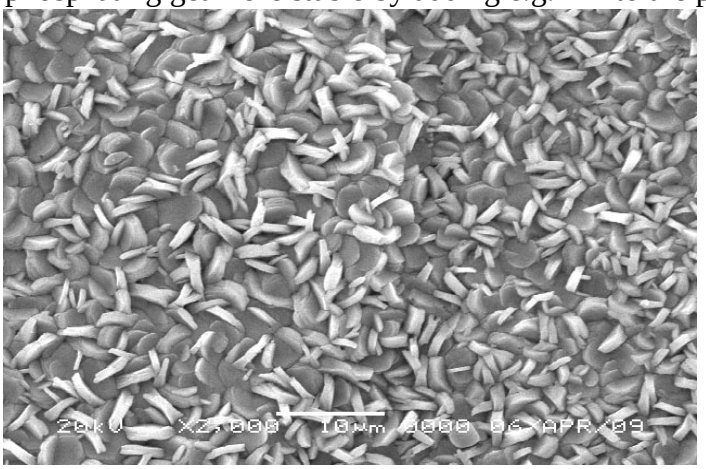

Figure 2.3. *SEM picture of a phosphating layer* [7].

### 2.2.2.2 Next Generations Pretreatments

Phosphating has been widely used in the automotive industry over the past decades before application of organic paints to achieve corrosion protection. There is a need to produce environmentally friendly pretreatments due to the environmental impact the phosphating process cause. There are environmental issues with the nickel containing trication phosphating process. The main driving force to replace the phosphating process is the risk that nickel will be classified as toxic. Another factor to consider is that an increased amount

of light weight metals in the automotive will poison the phosphating process. Aluminum for example produces a lot of sludge in phosphating baths which will affect the finish of the painted sheets.

There are also some additional drawbacks from energy and process standpoints; the existing method used today is highly water and energy demanding. As a consequence of these growing concerns new pretreatments technologies have been developed. Two kinds are of greatest interest, the zirconium based one and the silane based one. These ones will be described below [8,11] .

**Zirconium based pretreatments**

Zirconium based conversion coatings are investigated to work as new surface pretreatments. The process can be applied by spray or immersion and the commercially available pretreatment used today is based on hexafluorozirconic acid [12]. The coating is formed by electrochemical reactions including anodic- and cathodic sites. The metal substrate is oxidized and dissolved at the anode. Simultaneously $H^+$ is reduced at the cathode resulting in an increased pH. This causes the hexafluorozirconate to precipitate as zirconium dioxide on the substrate (Fig. 2.3). The coating consists mainly of zirconium oxide, substrate metal ions and various additives [13]. The weight is approximately 10-300 mg/m$^2$ (which is 10-100 times lower than for the traditional phosphating used today) [8] and the thickness roughly 20-50 nm [11]. Examples of zirconium based conversion coatings are TecTalis® and Zircobond® [13].

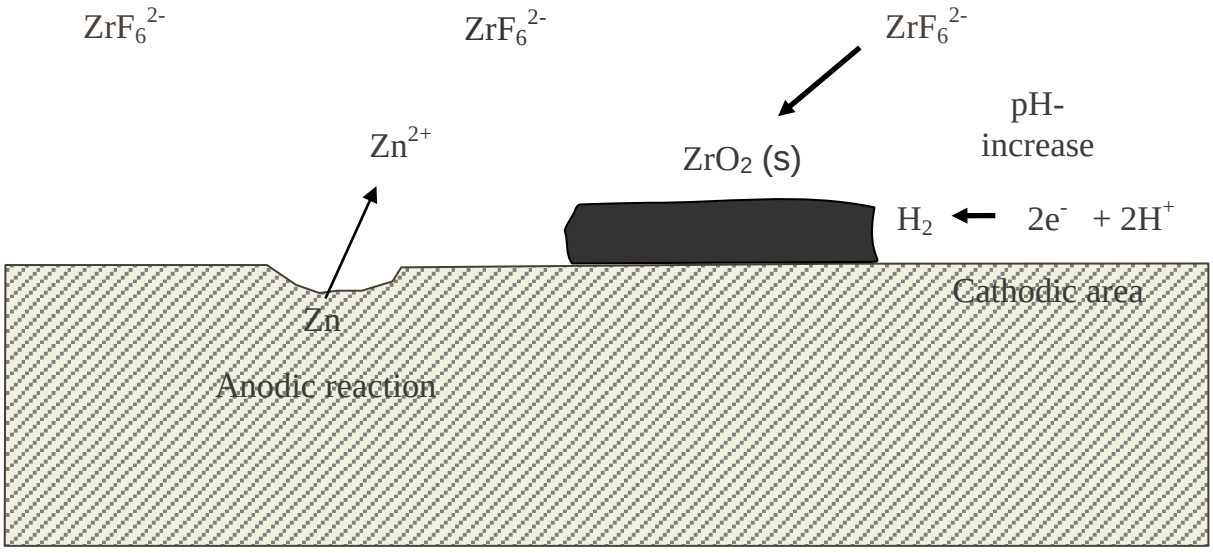


Figure 2.3. *General figure over the zirconium oxide formation* [7].

**Silane based pretreatments**

Silanes are a category of silicon hydrides with the general structure of Si-$X_4$. Examples are gamma- aminopropyltriethoxysilane, gamma-APS, and 1,2-bis(triethoxysilyl)ethane, BTSE.

| | |
|---|---|
| [-NH-$(CH_2)_3Si(OC_2H_5)_3$] | gamma-APS |
| [-$CH_2$-O-$Si(OCH_3)_3]_2$ | BTSE |

The silane layer is built up by two steps forming a network with strong Me-O-Si-R bonds (Eq. 2.2-2.3). A strong chemical bond is formed between the metal and pretreatment.

Siloxanes are hydroxylated in an organic solvent (Eq. 2.2). The metal hydroxides present on the metal surface were formed during the initial degreasing step, which therefore is an important step for the silane based pretreatment. The metal hydroxides react with hydroxides from the siloxanes (Eq. 2.3) forming the important Me-O-Si-R bond:

$$R-Si-(OR')_3 \xrightarrow{hydroxylation} R-Si(OH)_3 + 3R'OH \quad (2.2)$$

$$R-Si(OH)_3 + Me-OH \xrightarrow{decomposition} R-Si(OH)_2-O-Me + H_2O \quad (2.3)$$

The siloxanes need to be able to bond to the paint coating therefore the R group in equation 2.3 must be coupled to a functional group e.g. amines. The layer thickness can be controlled by the concentration of the silane solution used from the start. No rinsing is needed after the procedure since the solvent is removed during the drying operation. Hydroxide groups on adjacent siloxane molecules condense during curing forming a high degree of cross links (Fig. 2.4) [14]. An exceptionally long curing time increases the cross links within the silane film forming a denser network and the interactions with the paint get more difficult. A careful consideration regarding curing time is therefore of highest importance. Previous corrosion testing has shown a risk of dissolution of silanes at the interface when exposed to an aggressive atmosphere which impairs the performance of the coating and weakens the adhesion ability. In similarity to the zirconium based pretreatment this coating is also much thinner than the traditional phosphating (~20-100nm). Examples of silane based pretreatments are OXSILAN® and E-CLPS® [15].

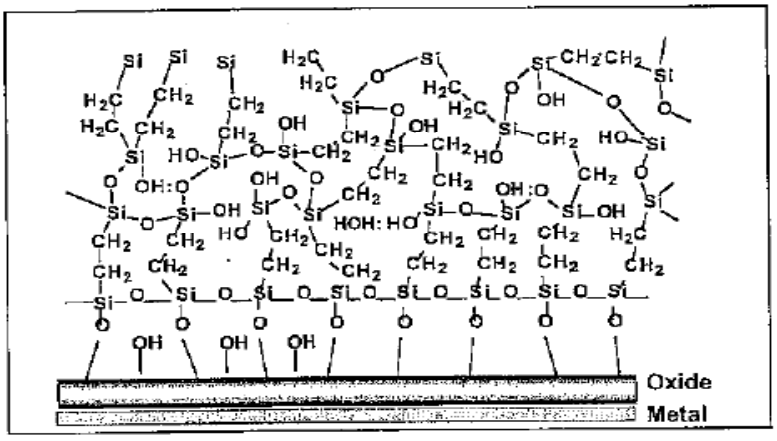


Figure 2.4. *Structure model of a silane layer* [14].

### 2.2.3 Organic Coating

The general organic coating system used at VCC in Torslanda is a four layer system (see fig. 2.1) where each layer contributes with different properties. The electro-dip (ED) coat is the first layer closest to the zinc layer providing the substrate with a main corrosion resistance and has a layer thickness of 18-20µm. On top of the ED coat is a primer surface (PS) which smoothens out the surface giving a flat structure. The PS coat provides the system with some colour and increases the mechanical stability. The base-coat (BC) brings colour to the product and provides some UV-protection as does the clear coat (CC). The main purpose of the CC coat, however, is to even out the surface and provide the final finish to the product. The CC coat also protects the BC coat mechanically [16].

## 2.3 Atmospheric Corrosion of Zinc

Corrosion of a painted car body panel can be considered as a special case of atmospheric corrosion. Since a lot of effort has been spent to understand the mechanisms of the

atmospheric corrosion of zinc, this topic will first be dealt with in this chapter. The second part will deal with the special case of corrosion of zinc under an organic coating.

Atmospheric corrosion proceeds at an appreciable rate only when it is of electrochemical nature. For this to occur, water in its liquid form has to be present. The corrosion rate is dependent of the kinetics of anodic/ cathodic processes, the conductivity of the electrolyte and the conductivity of the solid phase. Different air pollutants, relative humidity, temperature and weather changes are factors influencing the atmospheric corrosion [1].

The atmospheric corrosion can be categorized into rural, urban, industrial and marine types. The rural and urban areas both have little industrial activity. In the urban area however more $SO_x$ and $NO_x$ pollutions are present in the atmosphere. This is due to more motor vehicles related emissions. In the industrial area lots of air contaminants, e.g. Cl, $CO_2$, $SO_x$, $NO_x$ or $O_3$ are present. The marine atmosphere is a highly corrosive environment. High chloride content together with wind speed and direction carrying salt crystals from the oceans make these areas troublesome for corrosion protection [5].

### 2.3.1 General Aspects

The corrosion reactions of zinc if pollutants are absent are listed below.

Anodic reaction:

$$Zn(s) \rightarrow Zn^{2+} + 2e^{-} \qquad (2.4)$$

Cathodic reaction:

$$\tfrac{1}{2}O_2 + H_2O + 2e^{-} \rightarrow 2OH^{-} \qquad (2.5)$$

Zinc hydroxide is formed and precipitated as corrosion products on the surface (Fig. 2.5) [5]. If pollutants are present other cathodic reactions may be active [3].

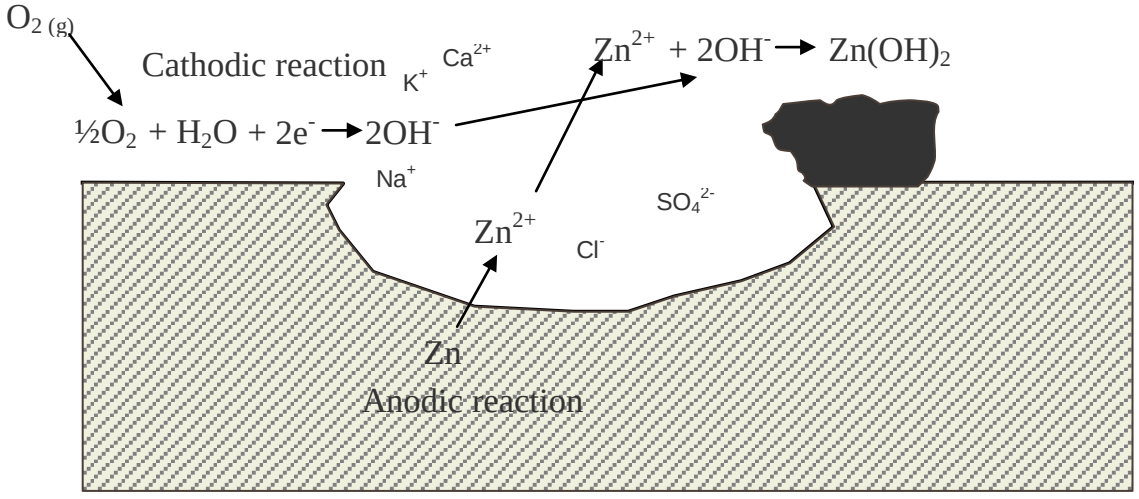


Figure 2.5. *Schematic picture of cathodic and anodic reactions at an initial stage* [7].

According to Amirudin the following events are possible. Zinc hydroxide is initially formed over the surface and retards the oxygen reduction due to the low electrical conductivity of zinc hydroxide. The zinc hydroxide is dehydrated into zinc oxide during dry cycle conditions. The zinc oxide is an n-type semiconductor and is a good catalyst for oxygen reduction. The consequence of this is an enhanced cathodic reaction rate [3].

The influences of air pollutants are also described by Amirudin and the common corrosion products are mentioned below. Carbonates are formed when carbon dioxide is present and are common compounds in atmospheric corrosion. When water and carbon dioxide in liquid form is in equilibrium, dihydrogen carbonate is formed (Eq. 2.6). The dihydrogen carbonate is in equilibrium with carbonate ions and its protons according to equations 2.7-2.8 [4,5]. The presence of carbonate in the electrolyte will result in the precipitation of zinc hydroxy carbonates (cf. equation 2.3). The most common carbonate containing corrosion products formed are hydrozincite [$Zn_5(CO_3)_2(OH)_6$] and smithsonite [$ZnCO_3$]. The hydroxy carbonates as well as the carbonates present in the electrolyte are believed to have a buffering effect and therefore offer corrosion protection [5].

$$CO_2(aq) \leftrightarrow H_2O \leftrightarrow H_2CO_3(aq) \quad (2.6)$$

$$H_2CO_3(aq) \leftrightarrow HCO_3^- + H^+ \quad (2.7)$$

$$HCO_3^- \leftrightarrow CO_3^- + H^+ \quad (2.8)$$

*Possible precipitation reaction for hydrozincite:*

$$Zn(OH)_2(s) + 4Zn^{2+} + 4OH^- + 2CO_3^{2-} \rightarrow Zn_5(CO_3)_2(OH)_6 \quad (2.9)$$

Sulphur dioxide present in the atmosphere in for instance rural areas dissolve into the surface film and gets oxidized into $HSO_3^-$. The presence of sulphate ion has been confirmed in corrosion layers by Odnevall [5,18]. Zinc hydroxychlorides are formed in a chloride environment, the most common one being simonkolleite [$Zn_5Cl_2(OH)_8*H_2O$]. Simonkolleite crystallizes in a hexagonal or a needle like pattern (Fig. 2.6). At a slightly higher pH [$Zn_7Cl_2(OH)_{10}* H_2O$] is formed but other, often metastable forms of zinc hydroxy chloride, are also possible [3, 19].

*Possible precipitation reaction according to Lindström:*

$$5Zn^{2+}(aq) + H_2O + 8OH^-(aq) + 2Cl^-(aq) \rightarrow Zn_5Cl_2(OH)_8 * H_2O(s) \quad (2.10)$$

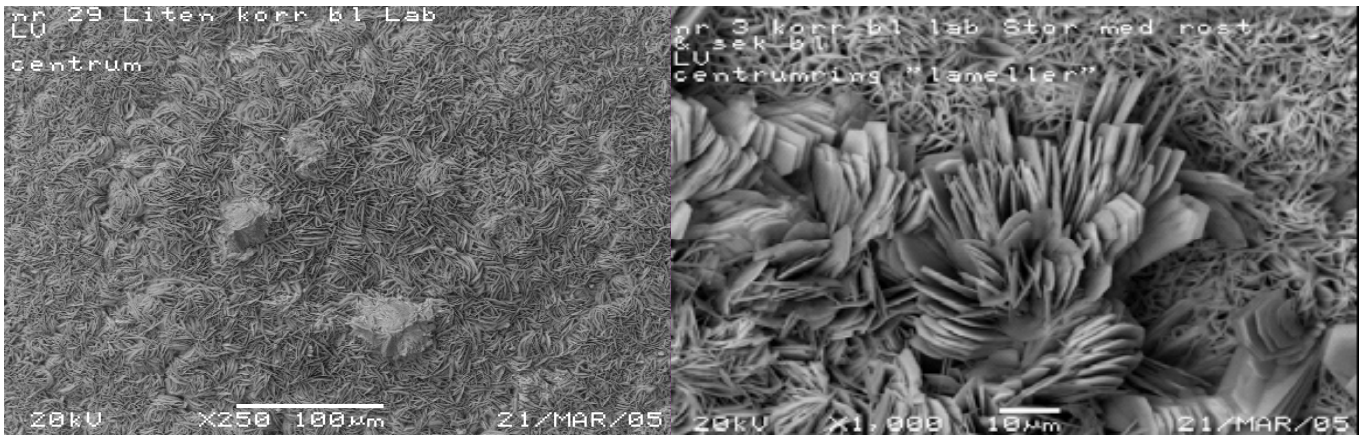


Figure 2.6. *SEM pictures of characteristic crystals of simonkolleite* [4]. *In the left picture the crystals are formed like needles and in the right picture as hexagonal plates.*

The equilibriums between zinc ions, simonkolleite and zinc oxide are pictured in a stability diagram made by Lindström (Fig. 2.7) [19]. The diagram predicts what compound that can be found at different pH and chloride concentrations. Every line in the diagram represents equilibrium and it can be seen that simonkolleite is formed at pH at around 5,5-8,5 and at fairly high chloride levels [17].

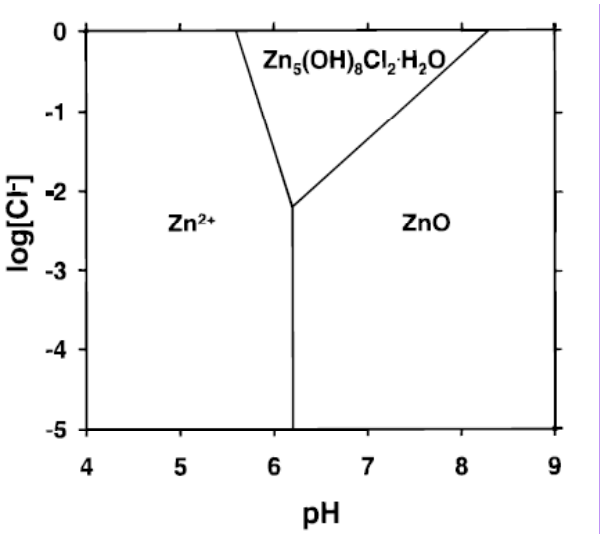


Figure 2.7. *Stability diagram, $[Zn^{2+}]$=0,1M at 25°C* [17].

The possible corrosion products detected with possible relevance to corrosion of zinc are listed in table 2.1. The corrosion products have been detected in various types of corrosive environments [20]. A complete list made by Graedel is listed in appendix.

Table 2.1. *Most common crystals containing zinc with possible relevance to the corrosion of zinc [*20].

| Substance | Crystal System | Formula |
|---|---|---|
| Zincite | Hexagonal | ZnO |
| Zinc hydroxide | Tetragonal | $Zn(OH)_2$ |
| Würtsite | Hexagonal | β-ZnS |
| Zinkosite | Orthorhombic | $ZnSO_4$ |
| Simonkolleite | Hexagonal | $Zn_5Cl_2(OH)_8*H_2O$ |
| Smithsonite | Trigonal | $ZnCO_3$ |
| Hydrozincite | Monoclinic | $Zn_5(CO_3)_2(OH)_6$ |
| Zinc nitrate | - | $Zn(NO_3)_2$ |

### 2.3.2 Blister Corrosion

Corrosion blisters is a cosmetic paint problem occasionally occurring in the car industry. It is a problem appearing where there is a mechanical defect in the paint coating on zinc covered steel exposed to a wet mud film containing salt. The size and number of blisters increase with time. In a previous study by Svensson [4] concerning blister corrosion it was found that the most existent corrosion product was simonkolleite. The initial formation of the blister happens when the electrolyte reaches the zinc layer through a defect in the film. A galvanic cell is formed once the zinc layer is in electrochemical contact with an external cathode through the electrolyte. Oxygen reduction takes place at the external cathode and zinc dissolution at the anode. The secondary blister is suggested to be formed by mechanical stresses at the periphery of the first blister [4].

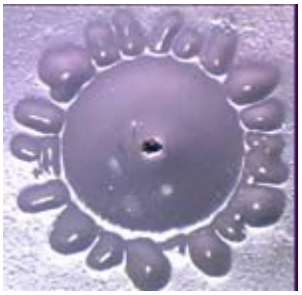

Figure 2.8. *A spherical corrosion blister with secondary corrosion, size ø4-5 mm* [4].

### 2.3.3 Filiform Corrosion

Filiform corrosion is a localized corrosion phenomenon that affects painted metals and occurs under atmospheric conditions usually when there is a surface defect in the protective film. The corrosion is characterized by long threadlike filaments delaminated in tracks (Fig. 2.9). The most common case is related to anodic delamination, which is described in more detail in chapter 2.5.1 [18].

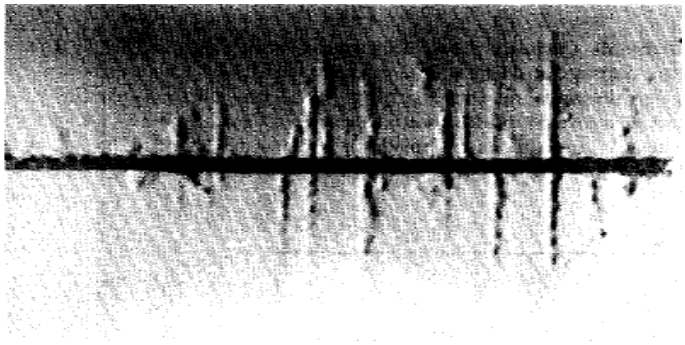

Figure 2.9. *Characteristic appearance of filiform corrosion* [24].

The filaments consist of a head and a tail, where the anodic head is working as an active corrosion cell and the cathodic tail is formed by corrosion products (Fig.2.10) [21].

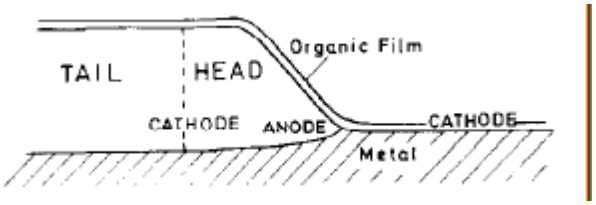


Figure 2.10. *Anodic and cathodic sites in filiform corrosion* [21].

## 2.4 Mechanisms of Paint Delamination

There is a relatively small amount of studies that deal with the subject of corrosion beneath an organic paint system. Marcus and Amirudin discuss two mechanisms for under paint corrosion; anodic delamination and cathodic delamination [2,18].

### 2.4.1 Anodic Delamination

Anodic delamination is a process causing dissolution of metal under the paint film. The anodic front is propagating under the paint coating with a defect in the paint acting as a cathode.

In the galvanic cell the anions (e.g. chloride ions) migrate to the anode and cations (e.g. sodium ions or zinc ions) to the cathode. The defect in the panel makes it easier for anions to

diffuse to the anodic site. The anodic front is moving forward and new anodic sites are formed ahead of the other. The zinc corrosion products take up more space than the original zinc layer and this expansion result in stresses at the pretreatment-metal interface and the delamination can therefore be a mechanical effect [2,18].

### 2.4.2 Cathodic Delamination

A cathodic front, with a high pH (about 10-14) is propagating under the coating causing disbondment between the paint coating and substrate. The mechanism is described by Amirudin.

For both the anodic- and the cathodic delamination the blister is in the nature of a differential aeration cell (Fig. 2.11). Oxygen diffuses through the paint coating. The anodic reaction takes place in the center of the aeration cell as pictured below (see fig. 2.11). Corrosion products are precipitated due to drying of corrosion sites. The precipitated corrosion products form a wedge which opens up the paint/ metal interface allowing oxygen to enter at the corrosion front. This is where the cathodic reaction takes place and thus the cell separates the anode and the cathode. [2,3,18].

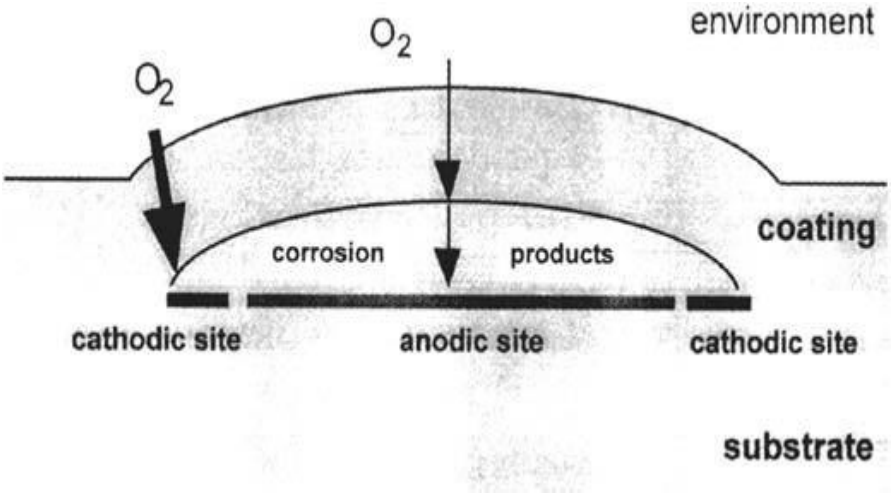


Figure 2.11. *Aeration cell* [5].

## 2.5 Factors Influencing Corrosion on Painted Zinc Coated Steel

There are a number of possible factors influencing corrosion of automotive materials e.g. type of metallic coating, coating thickness, pretreatment, organic coating, adhesion between paint and metal and exposure conditions. The metallic coating offer galvanic protection to the steel and depending on the type of coating a longer protection can be offered. Amirudin [3] relates the beneficial influence on corrosion resistance on phosphated substrates to better paint ability or lower reactivity of phosphated surfaces.

The exposure conditions differ depending on different corrosion test with the categories being standard neutral salt spray test, cyclic tests and atmospheric exposure. The different test conditions have various effects on the cosmetic corrosion [3].

# 3 Experimental

## 3.1 Test Panels

Samples prepared from panels of hot-dip galvanized steel with a size of 100*200 mm were used in this study. The different pretreatment systems, electro coats and basecoats used are stated in table 2.2. The table also indicates the exposure methods the different panels (marked A –G) have been subjected to. The thickness of the coating systems is ~130µm including zinc layer and consist of:

- Pretreatment layer
- Electrocoat layer
- Primer surface anthracite grey
- Basecoat
- Clearcoat

Material D is an exception where the only coating system is a polyester powder on top of the ED coating. The total coating layer being 101±10µm with zinc layer included.

Table 2.2. *Samples in the study. Their coating systems and exposure methods.*

| | **Pretreatment** | **ED coating** | **Basecoat** | **Exposure Method** |
|---|---|---|---|---|
| A1 | Phosphating Gardobond 2600+passivation Gardolene D6800/6 | BASF Cathoguard 350 | Black | ACT II |
| A2 | Phosphating Gardobond 2600+passivation Gardolene D6800/6 | BASF Cathoguard 350 | Silver metallic | ACT II |
| B | Silane based | BASF Cathoguard 350 | Black | ACT II |
| C | Zirconium based | BASF Cathoguard 350 | Black | ACT II |
| D | Silane based | PPG Enviroprime 2000 | Solid yellow powder | ACT II(6v) Drying CTS+salt spray |
| E | Phosphating Gardobond 2600+passivation Gardolene D6800/6 | BASF Cathoguard 350 | Black | Field exposure |
| F | Silane based | BASF Cathoguard 350 | Black | Field exposure |
| G | Zirconium based | BASF Cathoguard 350 | Black | Field exposure |

Panel E-G was cut in half before exposure. Two different panels of material A, sample A1 and A2, were analyzed.

## 3.2 Testing

### 3.2.1 Mechanical Damage for Corrosion Test

The panels are applied with a defect to act as a initiation point for the corrosion, the defect being a scribe in the coating done according to VCS 1021,29- *Scribing of a surface coated test object and evaluation of the propagation from scribe when corrosion testing*. The scribe is made using a template and cuts all the way to the substrate through the coating and possible galvanizing layers. A picture of the template is attached in appendix [22].

### 3.2.2 Bending Test

In an attempt to evaluate adhesion properties a bending test was performed on some samples according to VCS 1024,2529- *Bending Test*. Cut panels is bent with the help of a mandrel and the coating fracture is analyzed [23].

### 3.2.3 Global Laboratory Accelerated Cyclic Corrosion Test

The ACT II test is intended to mimic proving ground test and should have a similar effect in salt load and climatic factors. The purpose is to allow evaluation of the corrosion resistance in metals. The laboratory test is cyclic and consists of repeated cycles of salt solution exposure, differences in humidity, temperature and drying. The test is a verification method with possibilities to qualify corrosion products, finishing processes, select materials and to perform quality control [2]. A more detailed description of ACT II is given in appendix.

### 3.2.4 Climatic Testing System

The climatic testing system is a temperature and humidity controlled chamber tuned to have the same cycles as ACT II without the salt solution exposure.

### 3.2.5 Salt Spray

Panel D is put in the climatic testing system and is sprayed manually once a day Monday thru Friday with 0,5% KCl solution for 5 weeks. This was made in an attempt to detect potassium in the EDS analysis, potassium traces indicate cathodic activity. Sodium, which is normally used in corrosion chambers, is hard to detect in the EDS.

## 3.3 Methods for analysis

### 3.3.1 Paint Removal

On some panels the coating was removed to get a better analysis of the corrosion products. This was done by immersing the panels in a solution of 1/3 TEA, triethanol amine and 2/3 NMP, 1-methyl-2-pyrrolidon and slowly heating the solution to $80^0$C. When all the paint was removed the samples were rinsed with 2-propanol and acetone.

### 3.3.2 Optical Microscopy

Two different microscopes, a metal microscope (AX70) and a stereo microscope (Wild Heerbrugg), were used in this study. Both are equipped with a CCD-camera connected to a digital camera. The instruments were used to chart the samples to ease the SEM analysis.

### 3.3.3 Scanning Electron Microscope

A scanning electron microscope, SEM, connected to an energy dispersive X-ray, EDS, detector was used to analyze the topography, morphology and composition of the samples. The instrument used was a low vacuum SEM JSM-5600LV with a W-filament. This

technique is ideal for imaging and has a high depth of focus. The SEM can operate down to 50-100 nm and has a resolution in the range of 0.5-1 nm.

The principle underlying the SEM is obtaining information by electron beam irradiation. A focused electron beam bombards the sample creating different interactions between electron beam and the atoms in sample resulting in various kinds of information. The different emissions are collected in different kinds of detectors and provide different kinds of information. The secondary electrons give the highest resolved topographical images and the backscattered a compositional observation. The SEM operates in vacuum and the sample has a requirement of being conductive otherwise there will be a charge build up and the image can be distorted. Therefore non conductive samples must be coated with carbon or gold [24]. A way to overcome the requirement of having conductive samples is to operate the SEM in low vacuum mode. However the quality of the images is somewhat reduced when using low vacuum.

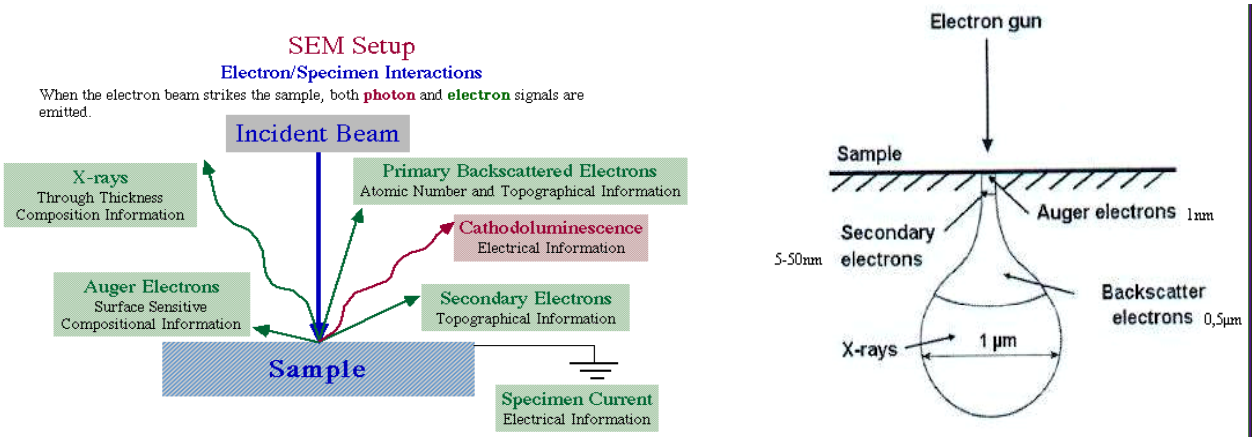


Figure 2.12. *Electrons active in SEM analysis.* [27, 25]

The droplet pictured above (Fig. 2.12) shows the size and depth of excitation which is determined by the acceleration voltage of the microscope, in this study ranging between 8 and 20 kV. By altering the acceleration voltage the analyzing depth of sample can be changed. A higher acceleration voltage goes deeper into the sample however the quality of the image is somewhat reduced [25].

### 3.3.4 Energy Dispersive X-ray Spectroscopy

The X-ray emissions from the bombardment of a primary electron beam are used to get an elemental analysis of the sample. The energies of the characteristic x-rays emitted are unique to each atomic element and can therefore be used to obtain compositional information in the sample [26].

An important aspect to remember while maneuvering the instrument is that the quantisation is only valid for even surfaces. A less topographic surface will give a better result. This effect is most pronounced for lighter elements. The lightest elements cannot be detected in the analysis; only elements from boron and above are possible.

### 3.3.5 Fourier Transform Infrared Spectroscopy

The instrument used in this study was Spectrum BX II equipped with an ATR (Attenuated Total Internal Reflection) crystal made out of zinc selenide, ZnSe. Fourier Transform Infrared Spectroscopy, FTIR is used to identify compounds by detecting functional groups. This is done by measuring the absorbance of IR light versus wavelength. The vibrations are related

to specific bonds and each bond vibrates at certain frequencies. This makes FTIR usable as a molecular fingerprint [26].

### 3.3.6 pH- Indicator

Phenolphthalein is used as a pH- indicator to detect acids and bases. If the environment is basic phenolphthalein will show pink colour and this indicates cathodic activity. The method was used in this study in an attempt to identify cathodic areas.

# 4 Result

## 4.1 ACT II exposed panels with different pretreatments

This chapter includes the results from ACT II exposed panels. The purpose with this investigation is to obtain information regarding corrosion mechanisms active correlated to different pretreatments. Panels with three different pretreatments are evaluated in this section; phosphated panels and silane- and zirconium based pretreated panels. This is done in an attempt to see if there is any differences in corrosion mechanism or corrosion spread for the different pretreatments.

### 4.1.1 Phosphated panels

Two different panels, sample A1 and A2, were analyzed both with the same coating system; A1 with black basecoat and A2 with silver metallic basecoat. A microscope picture of two corrosion blisters on sample A1, (phosphated panel) is shown in figure 4.1. In the left picture the two blisters are seen surrounded by smaller secondary blisters. This appearance, with smaller blisters surrounding the larger ones, is characteristic for phosphated samples. In the right picture the coating has been removed and it is possible to see tendencies to semi circular features; a growth ring formation. The arrow in figure 4.1 points out the semi circular pattern.

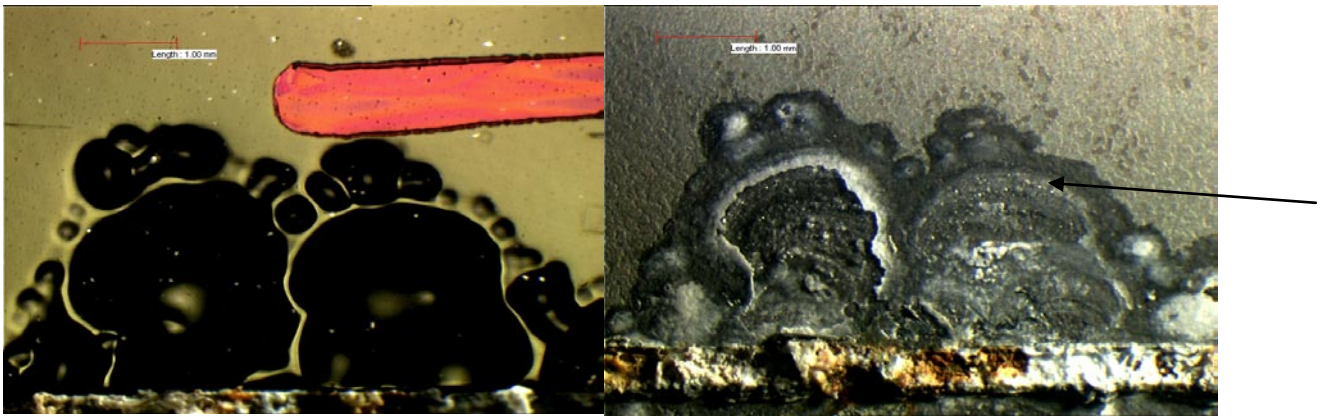

Figure 4.1. *Corrosion spreading on material A, A1. The scribe is in both pictures at the bottom of the picture. The left picture is with coating and in the right picture the coating has been removed.*

The left picture in figure 4.2 shows the substrate side on another phosphated sample A2, with a paint flake peeled off. The area where the flake has been peeled off represents the area under a blister. The right picture shows the corresponding backside of paint that has been peeled off. The same tendencies to growth ring formation are seen in both microscope pictures in figure 4.2 as seen in the right picture in figure 4.1. The left picture is marked with number 1-3 and the right picture is marked with letter A-C. The markings represent analyzing spots which is used in tables 4.1-4.4 below.

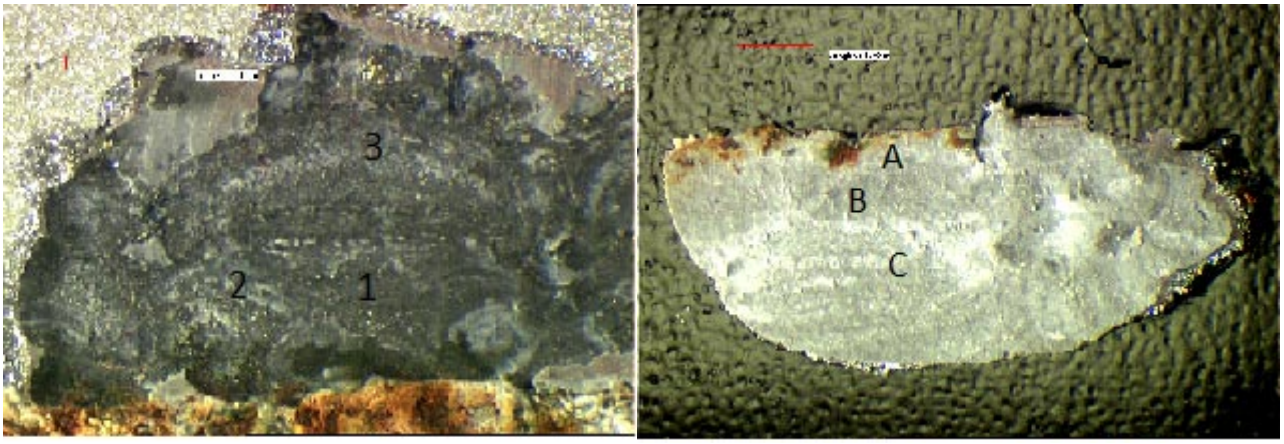


Figure 4.2. *The paint coating is peeled off and both the backside of the paint coating (right) and the metal substrate (left) is analyzed. The numbers indicate the analyzing spots. Sample A2.*

All samples were analyzed with SEM/EDS analysis. Figure 4.3 is a SEM picture from backside of paint from position A (marked in Fig. 4.2). In the picture thin needle like crystals are seen. EDS analysis (Tab. 4.1) shows highly chlorine containing corrosion products.


Figure 4.3. *SEM picture from backside of paint position A. Needle like crystals are seen.*

Figure 4.4 is a SEM picture from backside of paint position B (marked Fig. 4.2). In the picture a pattern from the backside of the phosphate crystals is seen. Hardly any corrosion products are seen. The EDS analysis (Tab. 4.1) shows a rather high phosphorous atomic composition and elements from the coating. In other words, the phosphate layer seems to be attached to the paint side of the fracture in a more or less intact form.

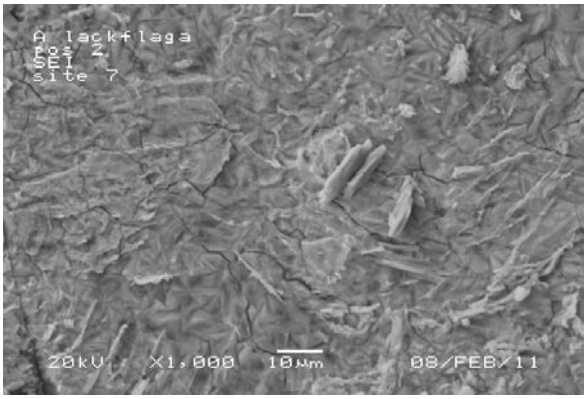


Figure 4.4. *SEM picture from backside of paint of material A, sample A2, position B.*

Figure 4.5 is from position C (marked in Fig. 4.2) backside of paint flake. The SEM picture shows thicker and bigger crystals if compared to the needle shaped crystals in figure 4.3. The crystals in SEM picture (Fig. 4.5) are more shaped like hexagonal plates. The EDS analysis (Tab. 4.1) shows in conformity with EDS analysis from position A highly chloride containing corrosion products.

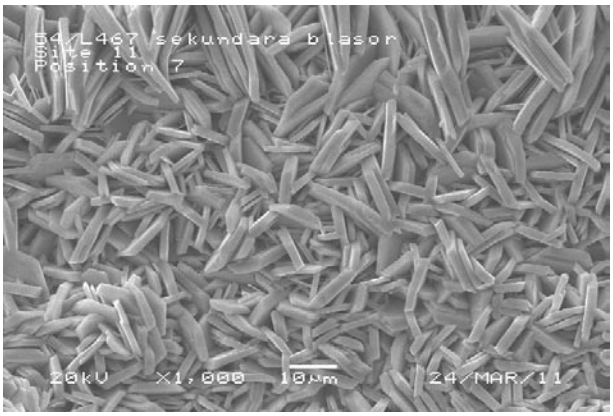


Figure 4.5. *SEM picture from backside of paint position C. The crystals are formed as hexagonal plates.*

Table 4.1 shows the result from EDS analysis from the backside of paint, position A-C (positions are marked in Fig. 4.2). The values represent the atomic composition for every element present in the sample.

Table 4.1. *Atomic composition for material A, sample A2, backside of paint , 20kV.*

| Position | Crystal shape | C | O | Al | Si | P | Cl | Ti | Mn | Fe | Ni | Zn |
|---|---|---|---|---|---|---|---|---|---|---|---|---|
| A | Needles (Fig. 4.3) | 21,32 | 38,42 | 0,31 | | | 9,24 | 1,25 | | 4,11 | | 25 |
| B | Phosphate crystal backside (Fig. 4.4) | 33,94 | 46,9 | 0,87 | 1,14 | 3,08 | 1,65 | 3,03 | 0,28 | 0,09 | 0,1 | 8,84 |
| C | Hexagonal plates (Fig. 4.5) | 22,11 | 54,71 | 0,19 | | | 6,25 | 0,2 | | | | 16,6 |

In table 4.2 calculated elements and ratios are shown. The zinc composition was corrected (Corr Zn) by removing the amount of zinc bound in the phosphate layer assuming that the zinc phosphate has the formula $Zn_3(PO_4)_2*4H_2O$. The corrected value zinc represents the amount zinc present in corrosion products. The oxygen composition was also corrected (Corr O). Oxygen is bound in oxides in the coating and in the phosphate. The corrected value represents what is present in the corrosion products. (It should be reminded, that due to the low energy of the oxygen Kα radiation, the quantification of oxygen is unreliable. This is also the case with carbon.)

Table 4.2. *Calculated ratios for material A, sample A2, backside of paint, 20kV (from table 4.1.).*

| Position | Corr Zn | Corr O | Zn/Cl | O/Zn | C/Zn |
|---|---|---|---|---|---|
| A | 24,96 | 29,30 | 2,70 | 1,17 | 0,85 |
| B | 4,22 | 18,60 | 2,56 | 4,42 | 8,04 |
| C | 16,55 | 54,00 | 2,65 | 3,26 | 1,34 |

The calculated Zn/Cl ratio is near 2,5 which is the ratio found in the zinc hydroxide chloride simonkolleite (Tab. 4.3). It is therefore proposed, that the corrosion product is mainly simonkolleite. Table 4.2 also shows that despite the different crystal sizes in position A and C the ratios are still the same.

Table 4.3. *Element ratios for simonkolleite and hydrozincite.*

| Ratios | Zn/Cl | O/Zn | C/Zn |
|---|---|---|---|
| Simonkolleite | 2,5 | 1,8 | - |
| Hydrozincite | ∞ | 2,4 | 0,4 |

The substrate was analyzed at an acceleration voltage of both 8 and 20kV and the atomic composition and calculated ratios are seen in table 4.4 and 4.5 respectively. The purpose of using 8 kV was to get a more surface sensitive analyze and thereby avoid contributions from the metallic substrate. The analysis is made on material A, sample A2, and on the substrate side. The analyzing spots, position 1-3, are pictured in figure 4.2.

Table 4.4. *Atomic composition for material A, sample A2, substrate side, 20 and 8kV.*

| Position | Crystal shape | C | O | Al | P | Cl | Fe | Zn |
|---|---|---|---|---|---|---|---|---|
| **20kV** | | | | | | | | |
| 1 | Hexagonal plates | 29,43 | 49,54 | 0,1 | 0,19 | 5,78 | 0,18 | 14,77 |
| 2 | Big needles | 28,63 | 37,56 | 0,26 | 0,35 | 7,37 | 0,45 | 25,38 |
| 3 | Small needles | 28,94 | 39,51 | 0,12 | 0,08 | 7,12 | 0,64 | 23,6 |
| **8kV** | | | | | | | | |
| 1 | Hexagonal plates | 18,86 | 46,9 | 0,02 | | 9,99 | | 24,22 |
| 2 | Big needles | 12,43 | 50,35 | 0,25 | 1,14 | 9,79 | | 26,03 |
| 3 | Small needles | 13,79 | 49,45 | 0,1 | | 10,65 | | 26,01 |

Table 4.5. *Calculated ratios for material A, sample A2, substrate side, 20 and 8kV (from table 4.4.)*

| Position | Corr Zn | Corr O | Zn/Cl | O/Zn | C/Zn |
|---|---|---|---|---|---|
| **20kV** | | | | | |
| 1 | 14,49 | 47,98 | 2,51 | 3,31 | 2,03 |
| 2 | 24,86 | 34,4 | 3,37 | 1,38 | 1,15 |
| 3 | 23,48 | 37,89 | 3,30 | 1,61 | 1,23 |
| **8kV** | | | | | |
| 1 | 24,22 | 46,87 | 2,42 | 1,94 | 0,78 |
| 2 | 24,32 | 43,14 | 2,48 | 1,77 | 0,51 |
| 3 | 26,01 | 49,3 | 2,44 | 1,90 | 0,53 |

The values from analysis with 20kV acceleration voltage on the substrate side of the fracture shows a higher Zn/Cl ratio (Tab. 4.5) than seen on the backside of the paint (Tab. 4.2). The values from 8kV however harmonize well with the ratio of the backside of paint and thus simonkolleite.

Figure 4.6 shows differences in crystal size and morphology. Position I in figure 4.6 represents the area from a growth ring. In this position the crystals are tiny, needle shaped and packed closely together. In position III which is slightly above position I in figure 4.6 the crystals are still needle shaped but somewhat larger than in position I. In position II however

the crystals are much larger than both in position I and III. The crystals in position II are shaped as hexagonal plates. The differences in crystal size will be discussed in chapter 5.1.6.

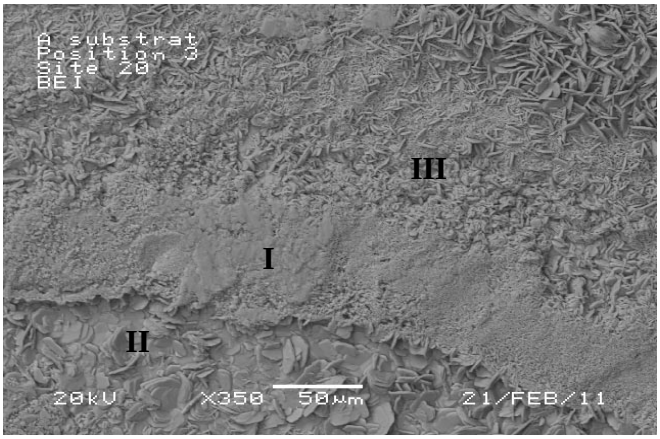


Figure 4.6. *SEM picture showing differences in morphology and crystal size, material A substrate side, sample A2. Area I is a growth ring.*

Despite the fact that the morphology and crystal sizes are different in figure 4.6; the EDS analysis gives the same result (Tab. 4.6). The iron signal in position II is higher compared to the position I and III (highlighted in table 4.6). This indicates that the signal from the substrate is high; probably due to the visibly thinner layer of corrosion products in position II.

The Zn/Cl ratio is rather high in all three positions compared to simonkolleite. An explanation could be that the corrosion product is a different type of zinc hydroxy chloride with a higher Zn/Cl ratio. Another explanation could be the presence of other zinc containing corrosion products e.g. hydrozincite. Corrosion products of this kind have been detected in studies made by Sabata [10].

Table 4.6. *EDS result from material A, sample A2, corresponding to figure 4.6, 20kV.*

| Position | C | O | Al | P | Cl | Fe | Zn | Corr Zn | Corr O | Zn/Cl | O/Zn | C/Zn |
|---|---|---|---|---|---|---|---|---|---|---|---|---|
| I | 32,39 | 37,47 | 0,05 | 0,26 | 6,82 | 0,41 | 22,60 | 22,21 | 35,22 | 3,26 | 1,59 | 1,46 |
| II | 14,84 | 43,99 | 0,1 | 0,27 | 6,96 | 1,34 | 32,48 | 30,08 | 40,21 | 4,61 | 1,25 | 0,46 |
| III | 19,17 | 46,46 | 0,08 | 0,28 | 7,00 | 0,56 | 26,46 | 26,04 | 43,82 | 3,72 | 1,68 | 0,74 |

FTIR analysis was performed on the backside of the coating and the result corresponds well with the SEM/EDS analysis. A piece of the backside of the coating from material A, sample A2, was mounted on the FTIR sample holder and analyzed. Figure 4.7 shows a difference spectrum of the sample. To obtain the difference spectrum the signals from ED coating and phosphate have been subtracted, by using reference spectrum for ED coating and phosphate. The remaining spectrum is in good agreement with simonkolleite. (A reference spectrum of simonkolleite is attached in appendix).

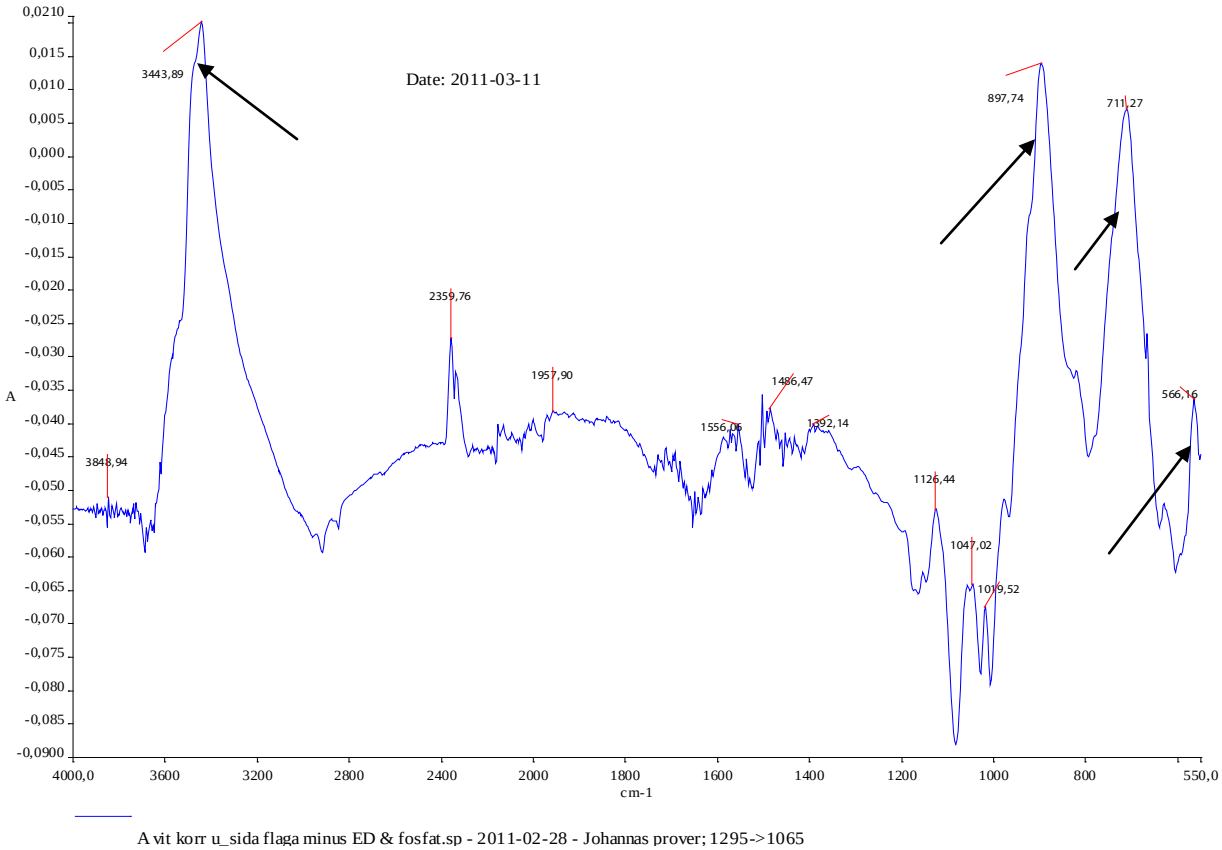


Figure 4.7. *Difference IR spectrum of material A from backside of paint.*

The most important peaks that are characteristic for simonkolleite are pointed out in figure 4.7.

A cross section of a corrosion blister on material A is shown in figure 4.8. The cross section of material A, sample A2, shows that the entire zinc layer, ~10µm, has completely corroded and there are no signs of any metallic zinc in the area under the blister (Fig.4.8).

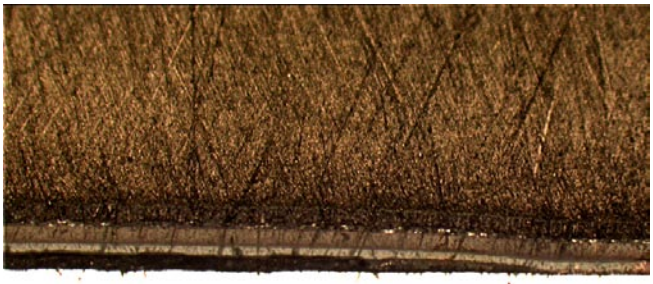

Figure 4.8. *AX70 Microscope picture of the cross section of a corrosion blister on sample A2.*

The front of the blister in cross section was analyzed with SEM. Figure 4.9 shows the front on one side of the blister and figure 4.10 the other side.

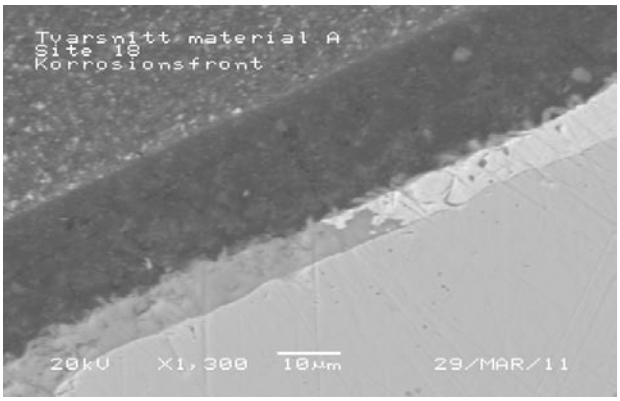


Figure 4.9. *The right side front of blister in cross section sample A2.*

In figure 4.10 it is possible to see a crack formation at the front of the blister. The crack stretches between the steel and the zinc layer. Taking into account that a considerable part of the zinc signal certainly originates from the metallic zinc layer, the EDS analysis rather indicates that simonkolleite is the corrosion product in the crack (see table 4.7). The analysis was made with 20kV and the zinc signal is quite high. The arrow points out the area analyzed.

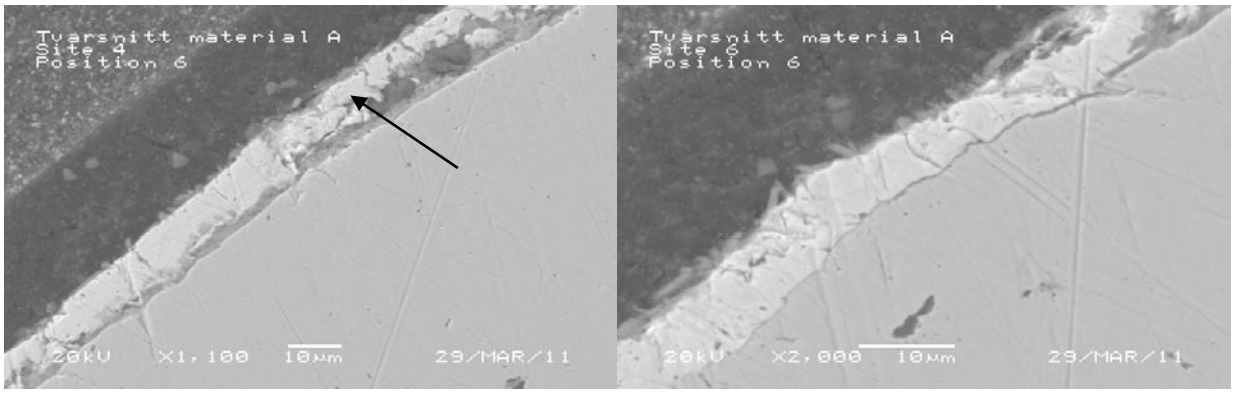


Figure 4.10. *The left side front of blister in cross section, material A, sample, A2. Beginning of crack formation (left) and continued crack (right).*

Table 4.7. *Atomic composition from crack in front of blister, 20kV (see Fig. 4.8)*

| C | O | Al | P | Cl | Fe | Zn | Si | Corr Zn | Corr O | Zn/Cl | O/Zn | C/Zn |
|---|---|---|---|---|---|---|---|---|---|---|---|---|
| 34,18 | 26,83 | 0,22 | 0,21 | 7,06 | 1,16 | 30,22 | 0.11 | 29,91 | 23,5 | 4,24 | 0,79 | 1,14 |

A SEM picture of the cross section of one corrosion blister from material A, sample A2, (phosphated) is shown in figure 4.11. The left picture shows the electron image of the cross section analyzed and the right picture shows the EDS mapping of phosphorous signal. The bright domains in the right picture indicate high amounts of phosphorous. An intact phosphate layer is seen after exposure. The bright domains are located above the crack and adjacent to the paint. This is in accordance with previous observations where phosphate crystals were seen to be attached to the backside of paint coating. Below the bright domains are the corrosion products. The corrosion spread seems to be in the zinc layer and the whole zinc layer seems to have corroded.

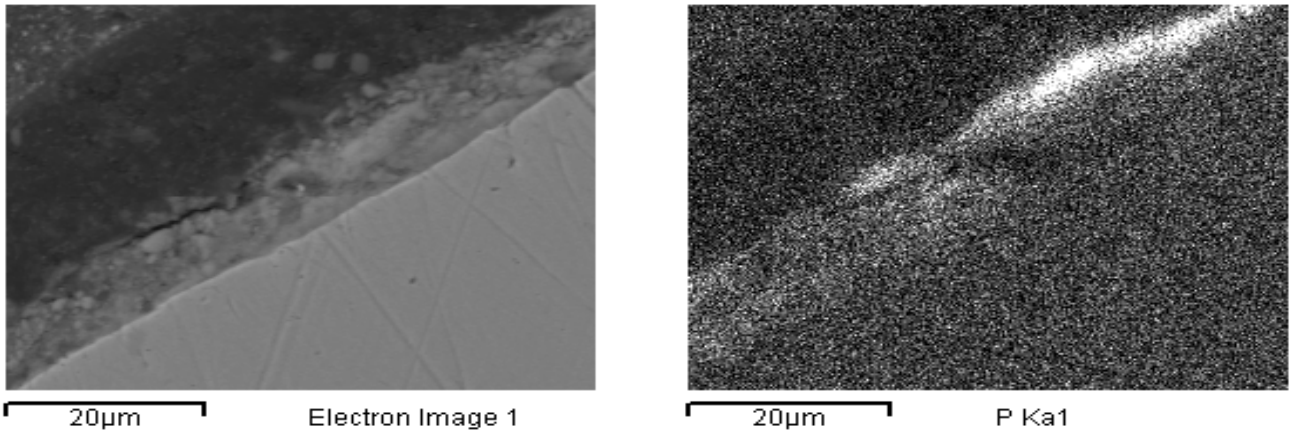


Figure 4.11. *The left picture shows the electron image of the cross section of material A, sample A2. The right picture shows the EDS element mapping of phosphorous.*

### 4.1.1.1 Analysis of the scribe

The scribe was analyzed by looking at the cross section of sample A2. Figure 4.12 shows a SEM picture from the analyzing area. The picture is only showing the scribe area of the sample. The arrow points out the analyzing spot.

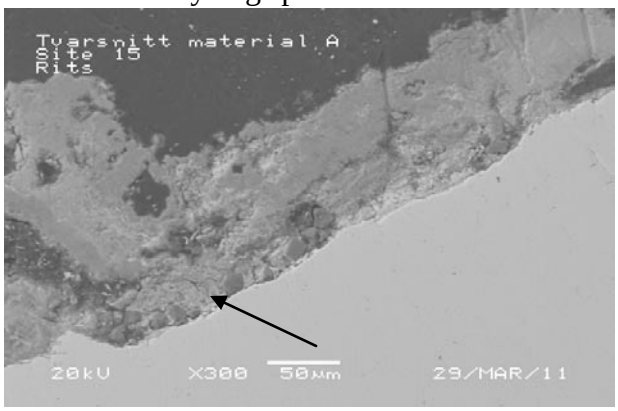


Figure 4.12. *SEM picture of a cross section of material A. The arrow shows the analyzing spot.*

Table 4.8 shows the EDS result from the spot pointed out in figure 4.12. The analysis shows that hardly any chloride is present. The result from the EDS analysis therefore indicates that zinc oxide is present in spot in the scribe. A considerable amount of the oxygen detected is bonded to the silicon; after subtracting this amount, the ratio O/Zn ≈ 1 as in ZnO.

Table 4.8. *Atomic composition from scribe, 20kV (see Fig. 4.11)*

| C | O | Al | Si | Cl | Fe | Zn |
|---|---|---|---|---|---|---|
| 60,06 | 21,06 | 0,03 | 4.75 | 0,1 | 1,03 | 12,97 |

### 4.1.1.2 Characterization of the phosphate layer under the paint coating

The phosphate layer was evaluated by looking at the morphology but also by performing a bending test. The bending test was made in an attempt to evaluate the adhesiveness of the pretreatment layer. The fracture during the bending test will take place at the weakest interface.

The morphology of the phosphated layer (after the paint has been removed) is clearly seen in SEM (Fig. 4.13). The phosphate crystals have full coverage over the surface.

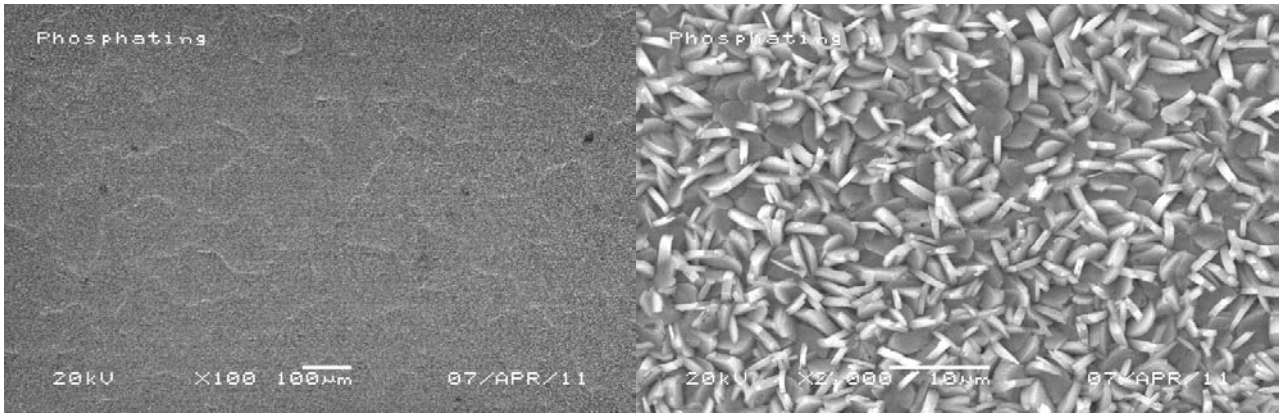


Figure 4.13. *SEM picture of phosphate layer, sample A2, after paint removal, 20kV.*

Figure 4.14 shows microscope pictures from after the bending test. The left picture below is from the substrate side and defect phosphate crystals are seen. The right picture shows the backside of the paint. In the microscope picture for the backside of the paint there are holes on the surface where phosphate crystals have been pulled out during the bending test.

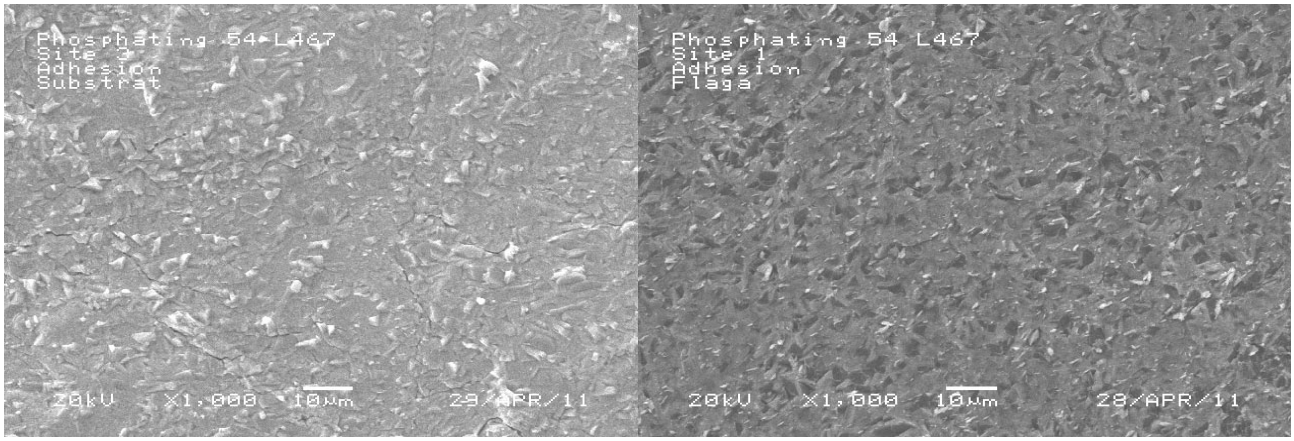


Figure 4.14. *SEM pictures from sample A2, with the substrate in left picture and the backside of paint in the right picture, after the bending test.*

The bending test showed tendencies of fracture within the phosphating layer (Fig. 4.14 and Tab. 4.9). Significant amounts from the phosphate layer are present on both backside of paint and on the substrate (see highlighted numbers in table 4.5). This observation indicates that the weakest interface observed from the bending test is within the phosphate layer.

Table 4.9. *Atomic compositions from EDS analysis of unexposed pretreated panels and exposed panels (material A, sample A2), 20kV.*

| **Pretreatment** | C | O | Al | P | Mn | Si | Fe | Ni | Ti | Zn |
|---|---|---|---|---|---|---|---|---|---|---|
| **Phosphating** | | | | | | | | | | |
| Unexposed (unpainted) | 8.81 | 47.76 | 0.37 | 8.91 | 1.45 | | | 0.29 | | 31.96 |
| Backside of paint. Material A (after bending test) | 45.02 | 42.47 | 0.39 | 3.26 | 0.72 | 0.52 | | 0.21 | 1.68 | 5.68 |
| Substrate side. Material A (after bending test) | 27.25 | 27.32 | 0.68 | 2.71 | 0.33 | | 0.12 | 0.12 | | 41.47 |

#### 4.1.1.3 Conclusions regarding phosphated panels

The evaluation of the phosphated panels leads to the following results. The main existent corrosion product found in the corrosion spread is simonkolleite. The corrosion takes place under the phosphate layer, on occasion between zinc and steel, and the whole zinc layer is consumed. The phosphate layer is attached to the backside of the paint after delamination. Zinc oxide is found in a specific spot in the scribe.

### 4.1.2 Silane Based Pretreatment

This chapter includes the results from evaluation of panels with the silane based pretreatment. This pretreatment is not only silicon based because it also contains e.g. zirconium hexafluoride and copper. In the EDS analysis zirconium, fluorine and copper work as indicators for the pretreatment. Two different panels are evaluated in this chapter, material B and D. The pretreatment for panel B and D are the same; however the coating system for the two panels is different (see table 2.2). Panel D was subjected to potassium chloride dosing instead of sodium chloride.

Figure 4.15 shows the corrosion spreading from the scribe on a painted panel with the silane based pretreatment, material B. The panel was exposed 6 weeks in ACT II. The shape of the blister in the figure below is different if compared to the blister on the phosphated panel. The blister in the picture below does not show any signs of secondary blisters and the shape of the blister is not as distinct as on the phosphated panel (Fig. 4.1). Figure 4.15 shows a less topographic corrosion blister compared to the phosphated sample. In the right part of the picture the paint film has been removed. A semi circular pattern, growth rings, is clearly seen. The growth ring pattern is more distinct than on the phosphated sample. The markings, number 4-6, in the right picture represent different analyzing spots, which is used in table 4.9.


Figure 4.15. *Corrosion spreading on material B. The scribe is in both pictures at the bottom of the picture. The left picture is with coating and in the right picture the coating has been peeled off. The markings 4-6 represent analyzing spots.*

Table 4.9 shows the result from the EDS analysis, 20kV, from the substrate side on material B, position 4-6 in figure 4.15. The analysis was performed in low vacuum mode in order to get a zirconium signal (otherwise, on gold sputtered samples, the Au signal interferes with the Zr signal). In the corrected zinc value (corr Zn) the zinc bounded in the pretreatment layer has been subtracted. The corrected oxygen (corr O) value represents what is present in the corrosion products. The bounded oxygen in coating is thus removed. The table shows highly chloride containing compounds in all positions. Table 4.3 shows highly chloride containing corrosion products with a Zn/Cl ratio 3,08-3,88. This indicates that the corrosion product found is a higher order of zinc hydoxy chloride.

Table 4.9. *Atomic composition and ratio calculations for material B substrate side, 20kV*

| Position | Crystal shape | C | O | Al | Si | Cl | Fe | Zn | Corr Zn | Corr O | Zn/Cl | O/Zn | C/Zn |
|---|---|---|---|---|---|---|---|---|---|---|---|---|---|
| 4 | Hexagonal plates | 22,57 | 44,18 | | | 7,95 | 0,55 | 24,74 | 24,74 | 43,36 | 3,11 | 1,75 | 0,91 |
| 5 | Needles | 27,68 | 37,59 | 0,23 | 0,12 | 6,91 | 0,45 | 27,02 | 26,84 | 35,85 | 3,88 | 1,34 | 1,03 |
| 6 | Needles | 26,49 | 38,38 | 0,53 | | 8,3 | 0,69 | 25,6 | 25,6 | 36,55 | 3,08 | 1,43 | 1,03 |

The backside of the paint peeled off from material B and corresponding to figure 4.15 was analyzed. The analysis was in conformity with the analysis above (Tab. 4.9) made in low vacuum mode. Table 4.10 shows the result from the EDS analysis. Significant amounts of zirconium are present on the backside of paint (highlighted in table 4.10). In table 4.9 on the other hand no zirconium was detected.

Table 4.10 *Atomic compositions for material B backside of paint, 20 kV.*

| C | O | Al | Si | Cl | Ti | Fe | Zn | Zr |
|---|---|---|---|---|---|---|---|---|
| 55.77 | 32.38 | 0.95 | 1.93 | 1.17 | 3.73 | 0.05 | 3.35 | 0.49 |
| 57.91 | 31.74 | 0.95 | 1.94 | 0.80 | 3.77 | 0.03 | 2.21 | 0.47 |

Table 4.9-4.10 indicate that zirconium only is present on the backside of the paint. The pretreatment layer is thus attached on the backside of the paint.

#### 4.1.2.1 Analysis of the Scribe

Two different attempts were made in order to localize the cathode. In the first attempt a pH-indicator, phenolphthalein, was used. Phenolphthalein is colorless in acidic environments and turns pink in basic. The basic environment is an indication of cathodic activity. Phenolphthalein was applied in the scribe on material D (Fig. 4.16) and in the corrosion spread in an area where the paint had been removed (not pictured).

Figure 4.16 shows a microscope picture of the scribe just after phenolphthalein had been applied. In the middle of the picture there is a pink spot. After this observation had been made the coating was removed. Phenolphthalein was applied in the corrosion spread. In the corrosion spread no color was seen.

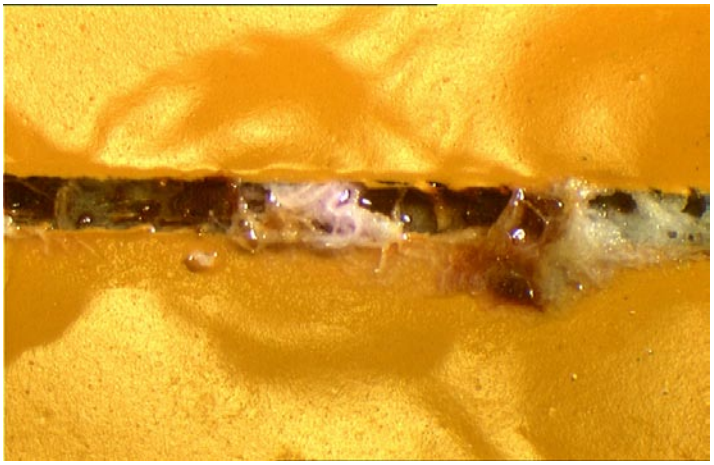

Figure 4.16. *Material D with applied phenolphthalein in the scribe.*

The pink colour in figure 4.16 indicates cathodic activity in that exact spot. No cathodic activity can be found in the corrosion spread.

In the second attempt material D was sprayed intermittently with potassium chloride for 5 weeks. In ACT II the panels are sprayed with sodium chloride, however sodium is hard to detect in EDS. Material D is therefore sprayed with potassium chloride instead in an attempt to localize potassium in EDS. Cations, in this case potassium ions, are attracted to the cathode. This attempt is thus made to find cathodic areas. The substrate side of material D was analyzed.

The result from the EDS analysis is shown in table 4.11. The atomic composition of potassium is highlighted. Three different positions are analyzed, near the scribe, close to scribe and at the front of the blister. The amount potassium is significantly higher near the scribe than close to the scribe. At the front of the blister no potassium was detected. A gradient of decreasing amount potassium is thus seen from near the scribe to the front of the blister.

Table 4.11. *Atomic composition material D substrate side, 20kV.*

| Position | C | O | Al | K | Ti | Fe | Zn | Si | Cl |
|---|---|---|---|---|---|---|---|---|---|
| Near scribe | 18.19 | 43.80 | 0.32 | 8.05 | 0.17 | 0.34 | 29.13 | | |
| Close to scribe | 19.79 | 63.44 | 2.11 | 0.77 | 0.13 | 0.08 | 11.82 | 1.50 | 0.35 |
| Front | 23.23 | 47.07 | 0.38 | 0 | | | 22.58 | | 6.73 |

The table (Tab. 4.11) clearly shows that the potassium is attracted to the scribe. This further proves that the cathode must be localized in the scribe. Hardly any potassium is found in the corrosion spread which indicates that the blister is the anodic site.

### 4.1.2.2 Characterization of the Silane Based Pretreatment Layer under the Paint Coating

An SEM/EDS analysis of the silane based pretreatment layer was made. The morphology of the silane pretreatment however is impossible to see in the SEM instrument used in this study. The pretreatment layer is too thin. A much higher magnification is needed to see the morphology of the pretreatment layer.

As with the phosphated panels a bending test was performed in order to assess the adhesiveness of the silane based pretreatment layer. Zirconium, fluorine and copper are used as indicators of pretreatment in this case; as mentioned in the beginning of section 4.1.2. There can be traces of silicon from the zinc layer and silicon is therefore not a trustworthy indicator for the pretreatment. Table 4.12 shows significant amounts of zirconium on both sides of the fracture (see highlighted numbers in table 4.12). Fluorine was not detected on the exposed substrate side, which may be due to that this signal is very weak and often overlapped with adjacent signals. No copper was detected. Table 4.12 shows in conformity with the phosphate layer tendencies to fracture within the pretreatment layer.

Table 4.12. *Atomic compositions from EDS analysis of unexposed pretreated panels and exposed panels after bending test (material B), 20kV.*

| Pretreatment | C | O | F | Al | Si | Fe | Ti | Zn | Zr |
|---|---|---|---|---|---|---|---|---|---|
| **Silane based** | | | | | | | | | |
| Unexposed (unpainted) | 8.03 | 16.89 | 1.51 | 1.38 | 0.25 | 0.31 | | 69.85 | 1.79 |
| Backside of paint. Material B (after bending test) | 54.62 | 33.49 | 3.88 | 0.99 | 1.66 | | 3.46 | 0.79 | 0.69 |
| Substrate side. Material B (after bending test) | 22.12 | 10.48 | | 0.99 | | 0.50 | | 65.08 | 0.84 |

### 4.1.2.3 Conclusions Regarding Panels with Silane Based Pretreatment

The result from evaluation from the silane based pretreated panels seem to be well in accordance with the phosphate panel. The corrosion product found in the corrosion spread from both analyses is zinc hydroxy chloride, mainly simonkolleite. The cathodic area seems to be localized to a specific spot in the scribe. The pretreatment layer is attached to the backside of the paint coating after the delamination caused by corrosion in the cyclic lab tests.

What differs however is the shape of corrosion blister. The phosphated panel showed well defined blisters with secondary blister surrounding the larger one. On the silane based pretreated panel the blisters are less topographic compared to the phosphated sample and no secondary blisters are seen. The growth ring pattern is more clearly visible for the silane based pretreatment compared to the phosphated panels.

### 4.1.3 Zirconium Based Pretreatment

The result from the analysis of the zirconium based pretreated panel, material C, are presented in this chapter. Zirconium, fluoride and copper in the EDS analysis indicate the presence of this pretreatment.

Figure 4.17 shows the corrosion spreading from the scribe on a panel with the zirconium based pretreatment, material C. The shape of the blister is in accordance with the blisters on the silane based pretreated panels (Fig. 4.15) less topographic compared to the phosphated sample (Fig. 4.1). The blisters on the zirconium based sample (Fig. 4.17) are even more flat than the silane based (Fig. 4.15). No secondary blisters are seen.

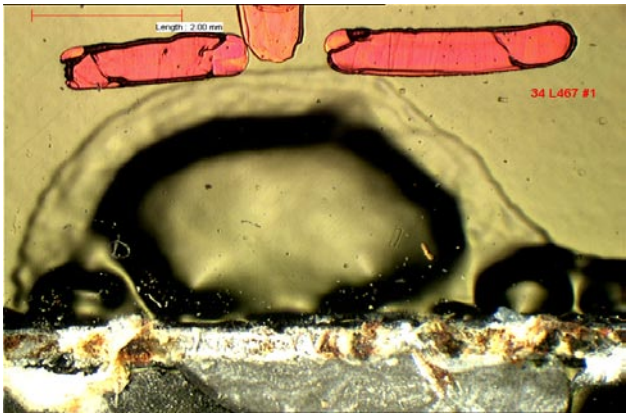


Figure 4.17. *Corrosion spreading on material C. The scribe is localized in the bottom of the picture.*

The paint film (seen in Fig.4.17) has been peeled off in the left picture in figure 4.18. Very distinct growth rings are seen and the number of semi circular rings is approximated to 20. The growth rings are most clearly seen on the zirconium based pretreated panel compared to the phosphated and the silane based pretreated panel. The numbers 7-8 are analyzing spots used in table 4.13. The right picture in figure 4.18 shows the backside of the paint flake. The paint flake corresponds to the peeled off flake from the left picture. Growth rings are clearly visible also on the backside of the paint.

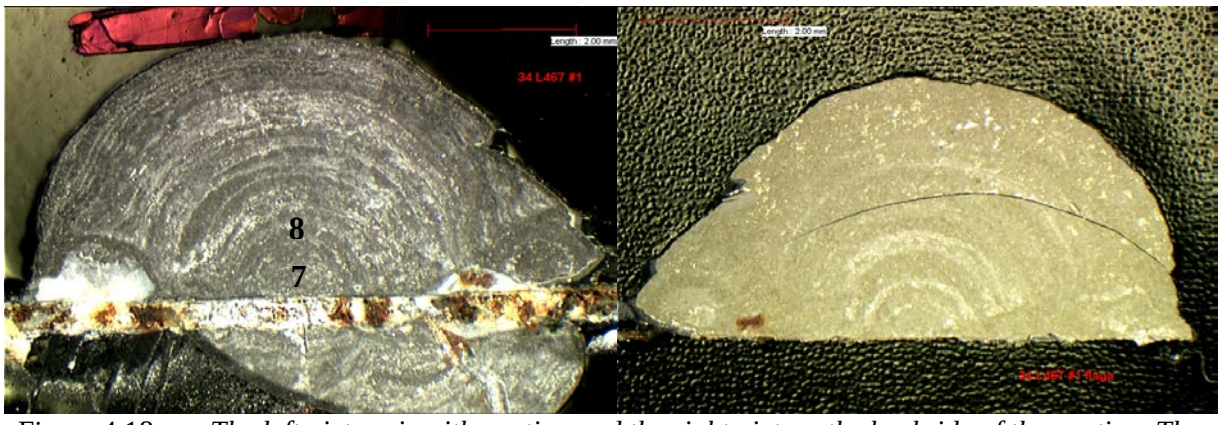


Figure 4.18. *The left picture is with coating and the right picture the backside of the coating. The scribe is in both pictures at the bottom of the picture. Sample C.*

Table 4.13 shows the result from the EDS analysis, 8kV and 20 kV, from the substrate side material C, position 7-8 in figure 4.18. The analysis was performed in low vacuum mode to be able to detect zirconium. The corrected values are calculated on the same basis as in

chapter 4.1.1 and 4.1.2. From the analysis with 20kV a rather high Zn/Cl ratio was detected. The corrosion product is a higher order of zinc hydroxy chloride. The 8kV analysis however shows a lower Zn/Cl ratio well in accordance with the ratio of simonkolleite (Tab. 4.3).

Table 4.13. *Atomic compositions and ratio calculations for material C substrate, 20 and 8Kv.*

| Position | Crystal shape | C | O | Al | Cl | Fe | Zn | Corr Zn | Corr O | Zn/Cl | O/Zn | C/Zn |
|---|---|---|---|---|---|---|---|---|---|---|---|---|
| **20kV** | | | | | | | | | | | | |
| 7 | Hexagonal plates | 16,32 | 45,9 | | 7,59 | 0,37 | 29,74 | 29,74 | 45,35 | 3,92 | 1,52 | 0,55 |
| 8 | Hexagonal plates | 24,45 | 38,43 | 0,61 | 8,68 | 0,61 | 27,22 | 27,22 | 36,6 | 3,14 | 1,34 | 0,90 |
| **8kV** | | | | | | | | | | | | |
| 8 | Hexagonal plates | 19,94 | 39,93 | | 11,07 | | 29,06 | 29,06 | 39,93 | 2,63 | 1,37 | 0,69 |

The backside of paint from material C, corresponding to the flake pictured in figure 4.18 was analyzed. The result from the analysis is presented in table 4.14. The analysis was made in low vacuum mode. Table 4.14 shows significant amounts of zirconium on the backside of the paint (highlighted in table 4.14). This can be compared to table 4.13 where no zirconium was detected on the substrate side of material C.

Table 4.14. *Atomic compositions for material C backside of paint, 20 kV.*

| C | O | Al | Si | Cl | Ti | Zn | Zr |
|---|---|---|---|---|---|---|---|
| 59.48 | 30.41 | 0.96 | 1.92 | 0.76 | 3.77 | 2.02 | 0.48 |
| 59.28 | 30.63 | 0.93 | 2.00 | 0.78 | 3.68 | 2.02 | 0.47 |

Table 4.13-4.14 shows that zirconium only is present on the backside of coating. The pretreatment layer is attached to the backside of the paint. This result is in conformity with the result from the previous analyses on the phosphate panel and the panel with silane based pretreatment.

FTIR was performed on a piece of the backside of the paint from material C. The analysis was made in the same way as described in chapter 4.1.1. Figure 4.19 shows a difference spectrum of the sample. In the spectrum the signal for the ED coating has been subtracted. The difference spectrum is in good agreement with simonkolleite and corresponds well with the results from SEM/EDS analysis. (A reference spectrum of simonkolleite is attached in appendix).

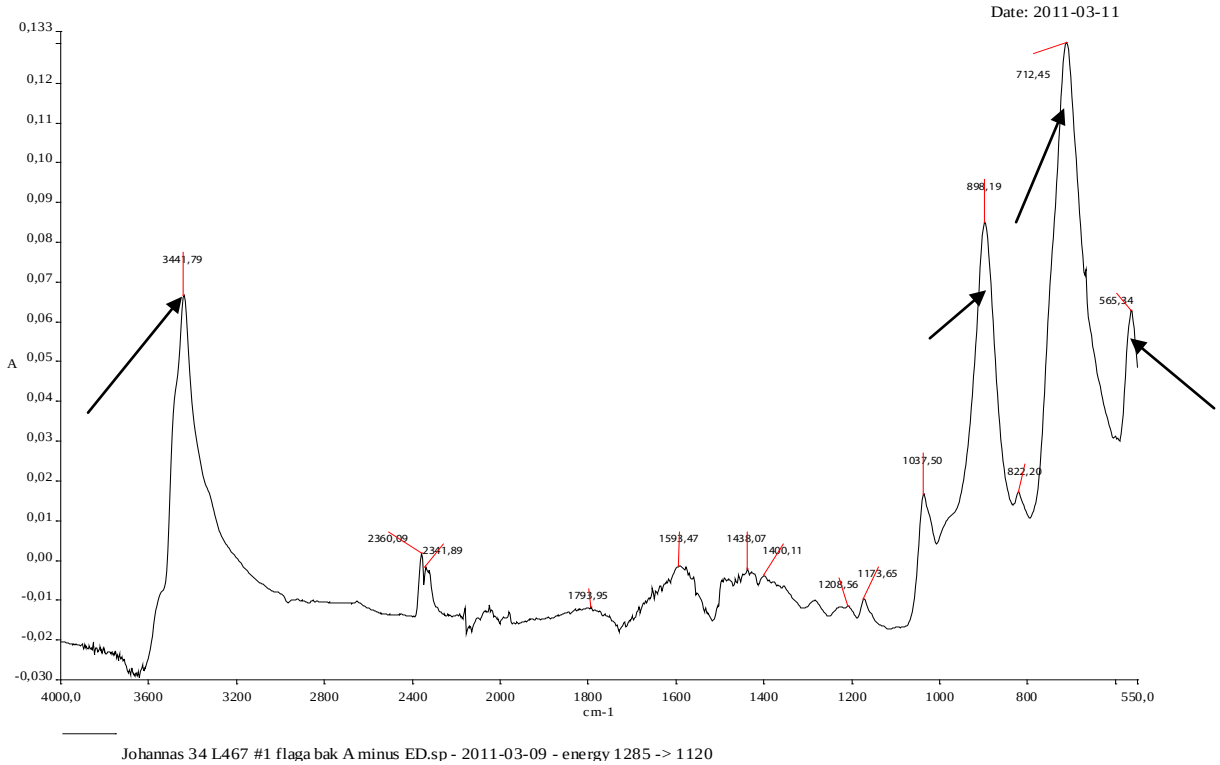


Figure 4.19. *Difference IR spectrum of material C from backside of paint.*

The most important peaks that are characteristic for simonkolleite are pointed out in figure 4.19. The difference IR spectrum is well in accordance with figure 4.7 (IR- spectrum from the silane based pretreated panel).

Figure 4.20 shows a microscope picture of the cross section of one corrosion blister from material C (zirconium based). The left picture shows the electron image of the cross section analyzed and the right picture shows the EDS mapping of zirconium signal. The bright domain in the left picture (see arrow in figure 4.20) indicates zirconium. Below the bright layer is the corroded zinc layer. The picture indicates that the corrosion spread is below the zirconium layer and that all zinc has corroded. The pretreatment layer, bright layer in figure 4.20, seems to stay intact after exposure.

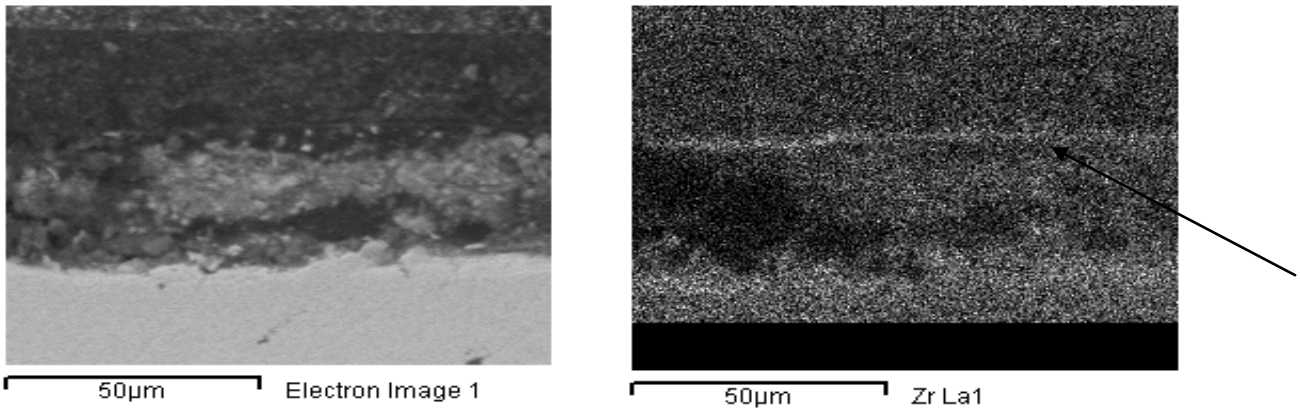


Figure 4.20. *The left picture shows the electron image of the cross section of material C. The right picture shows the EDS element mapping analysis of zirconium.*

### 4.1.3.1 Characterization of the Zirconium Based Pretreatment Layer under the Paint Coating

The zirconium based pretreatment layer was evaluated in a similar manner as the other two pretreatments. A bending test was performed on material C. Traces of zirconium in the EDS analysis indicate that the pretreatment layer is present. The morphology of the zirconium layer is impossible to see with the analyzing methods used in this study, in accordance with the silane based pretreatment layer.

A bending test was performed on material C in order to evaluate the adhesiveness of the zirconium based pretreatment layer to the paint coating. Table 4.15 shows significant amounts of zirconium on both backside of paint and on the substrate side (see highlighted numbers in table 4.15). Neither fluorine nor copper was detected on the exposed substrate side, which could indicate a weak and insecure EDS signal for that analysis. The result is in accordance with the result from bending test for the other pretreatments, i.e. the fracture during bending test seems to take place within the pretreatment layer.

Table 4.15. *Atomic compositions from EDS analysis of unexposed pretreated panels and exposed panels after bending test (material C).*

| Pretreatment | C | O | Al | Si | Fe | Ti | Zn | Zr |
|---|---|---|---|---|---|---|---|---|
| **Zirconium based** | | | | | | | | |
| Unexposed (unpainted) | 11.25 | 16.90 | 1.01 | | 0.38 | | 69.10 | 1.36 |
| Exposed backside of paint , material C (after bending test) | 61.85 | 29.80 | 0.91 | 1.98 | | 4.15 | 0.56 | 0.40 |
| Exposed substrate, material C (after bending test) | 37.87 | 7.70 | 1.03 | | 0.36 | | 52.69 | 0.35 |

### 4.1.3.2 Conclusions Regarding Panels with Zirconium Based Pretreatment

The corrosion product found in the corrosion spread on the zirconium based pretreated panel is a zinc hydroxy chloride, mainly simonkolleite. This corrosion product is found on all

panels, phosphated, silane based and zirconium based ones, evaluated in this study. Another result in well accordance on all panels is the intact pretreatment layer which stays attached to the backside of the paint after corrosion delamination.

The shape of the corrosion blister on the zirconium- and silane based panels is similar. The corrosion spread is rather flat and less topographic if compared to the phosphated panel. No secondary blisters are seen. There is a difference in distinction of growth rings between differently pretreated panels. The growth rings are less visible on the phosphated panel. On the silane based panel the growth rings are more distinct and on the zirconium based the growth rings are very clear and easy to see and even to count.

## 4.2 Field Exposure Panels

The panels evaluated in this section had been mounted underneath a truck which drove around in Western Sweden for one year's time. The purpose of this study was to see if the corrosion behavior was the same after field exposure and lab exposure. This is of greatest interest for the corrosion testing. The ideal situation is to get the same result and corrosion mechanisms from field exposure and lab exposure. Panels with three different pretreatments were analyzed; phosphated panels and silane and zirconium based pretreated panels. The corrosion spread from the field exposure was small (~1mm) compared to the ACT II exposed panels (~4-6mm). The panels from the field exposure were cut in half (as mentioned in section 3.1). The corrosion from both the scribe and the cut edge will be evaluated in this chapter. The evaluation of field exposed panels was not given as much time as needed in this study. More studies on field exposed panels need to be made.

### 4.2.1 Phosphated Panels

This section will present the result from the phosphated panel from the field exposure, material E. Figure 4.21 shows a microscope picture of the corrosion spread from the scribe of material E. A paint flake has been peeled off. The appearance of the corrosion blister is somewhat irregular compared to the samples exposed in ACT II (cf. fig. 4.1). However the blister still shows some tendencies to secondary blister formation. No growth ring pattern is seen. The scribe is more featureless compared to the lab exposed panel (see fig. 4.1).

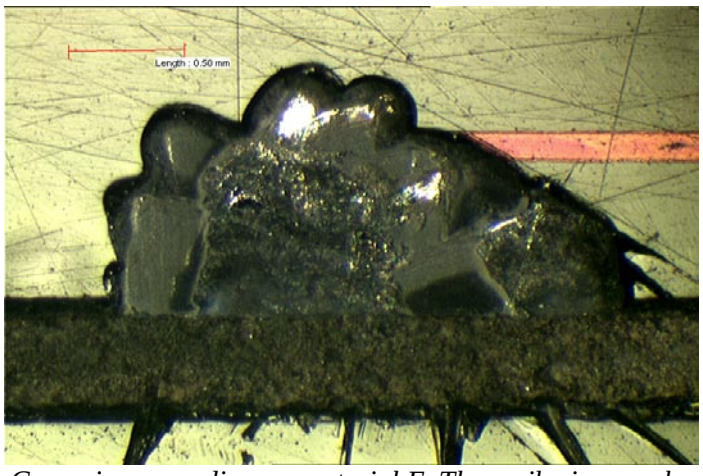


Figure 4.21. *Corrosion spreading on material E. The scribe is more homogenous than the lab exposed panel and is located in the bottom of the picture.*

Table 4.16 shows the EDS result both from the substrate side (pictured in figure 4.21) and the backside of the paint flake peeled off on material E. The corrected values (corr Zn and corr O) in table 4.16 are calculated in the same manner as described in chapter 4.1.1.

The Zn/Cl ratio is rather high (Zn/Cl=2,9-3,6) and indicates a higher order of zinc hydroxy chloride.

Table 4.16. *Atomic composition and ratio calculation from sample E, 20kV.*

| Position | Crystal shape | C | O | Al | P | Cl | Fe | Zn | Si | S | Corr Zn | Corr O | Zn/Cl | O/Zn | C/Zn |
|---|---|---|---|---|---|---|---|---|---|---|---|---|---|---|---|
| Substrate | Needles | 19,71 | 43,32 | 0,45 | 0,34 | 8,2 | 0,39 | 27,41 | 0,18 | | 26,9 | 40,02 | 3,28 | 1,49 | 0,73 |
| Substrate | Needles | 17,85 | 48,67 | | 0,34 | 7,79 | 0,32 | 24,87 | | | 24,36 | 46,15 | 3,13 | 1,89 | 0,73 |
| Backside of paint | Needles | 13,1 | 55,71 | 0,15 | 1,57 | 6,25 | | 20,45 | 0,17 | 1,64 | 18,1 | 46,07 | 2,9 | 2,55 | 0,72 |
| Backside of paint | Needles | 16,05 | 49,72 | 0,19 | 1,19 | 6,12 | | 23,61 | 0,14 | 1,8 | 21,83 | 42,3 | 3,57 | 1,94 | 0,74 |

Table 4.16 shows amounts of phosphorous on both backside of the paint and on the substrate side. No phosphate crystals are seen on the substrate side however the EDS analysis indicates traces of phosphorous. The result in table 4.16 indicates a fracture within the phosphate layer. However more studies and analysis need to be made in order to draw any conclusions regarding this observation.

The corrosion spreading from the cut edge on material E was analyzed. SEM pictures from the analysis are seen in figure 4.22. The left picture is from the substrate side of the phosphated panel from field exposure. The morphology in the left picture is similar to the morphology of phosphate pretreatment layer. The same morphology can be seen on the backside of the paint in the right picture in figure 4.22 (in the lower, darker part in the picture).

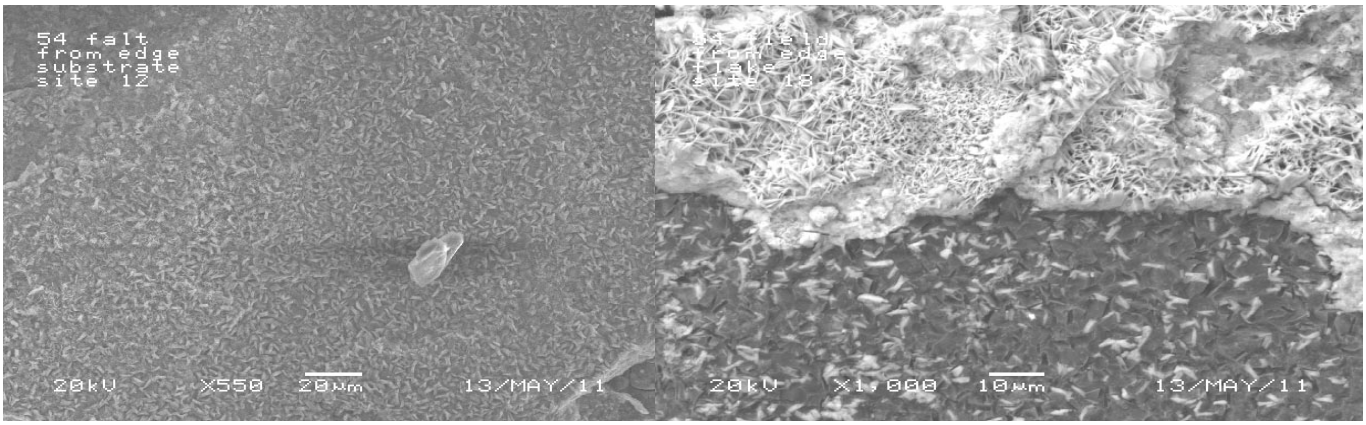


Figure 4.22. *SEM picture from backside of paint (right) and from substrate (left) sample E, 20kV.*

The area on the substrate side described in the section above, with morphology similar to the phosphate layer, is analyzed further. The EDS result is shown in table 4.17. The corrected values (Corr Zn and Corr O) are calculated in the same manner as described in chapter 4.1.1. No phosphorous was detected. The ratio Zn/Cl is rather high (compared to the Zn/Cl ratio of simonkolleite), however the analysis indicates that the corrosion product is a higher order of zinc hydroxy chloride.

Table 4.17. *Atomic composition of substrate in figure 4,22.*

| C | O | Al | Si | Cl | Fe | Zn | Mn | Corr Zn | Corr O | Zn/Cl | O/Zn | C/Zn |
|---|---|---|---|---|---|---|---|---|---|---|---|---|
| | | | | | | | | | | | | |
| 23,29 | 43,26 | 0,13 | 0,07 | 7,59 | 0,33 | 25,2 | 0,13 | 25,1 | 42,15 | 3,31 | 1,68 | 0,93 |

Table 4.18 shows the EDS result from two different areas than in figure 4.22; both the substrate side and the backside of the paint was analyzed. The ratio Zn/Cl from the substrate side is above 3 and indicates a zinc hydroxy chloride. However, the corrosion product on the backside of the paint is not chlorine containing. The corrosion product found on the backside of the paint on material E is therefore not a zinc hydroxy chloride. A suggested corrosion product is hydrozincite (Tab. 4.3).

Table 4.18. *Atomic composition and ratio calculation from edge sample E, 20kV.*

| Position | Crystal shape | C | O | Al | Cl | Fe | Zn | Si | Corr Zn | Corr O | Zn/Cl | O/Zn | C/Zn |
|---|---|---|---|---|---|---|---|---|---|---|---|---|---|
| Edge/backside of paint | Round features | 18,05 | 56,57 | 0,14 | 0,36 | | 24,46 | 0,03 | 24,46 | 56,36 | | 2,30 | 0,74 |
| Edge/substrate | Needles | 23,29 | 43,26 | 0,13 | 7,59 | 0,33 | 25,2 | 0,07 | 25,2 | 42,57 | 3,32 | 1,69 | 0,92 |

#### 4.2.1.1 Conclusions Regarding Phosphated Panels from Field Exposure

The most existent corrosion product is a zinc hydroxy chloride. A corrosion product without chlorine was detected on the backside of paint from the edge sample, possibly hydrozincite. The corrosion front seems to have wandered within the pretreatment layer, which is not the case for the lab exposed panels.

The shape of the corrosion blister is somewhat irregular if compared to the lab exposed phosphate panel. Tendencies to formation of secondary blisters are seen. No growth rings are seen. The scribe is featureless.

### 4.2.2 Silane Based Pretreatment

The analysis result from the panel with silane based pretreatment, material F, from field exposure are presented in this chapter. The panel is evaluated from scribe and from the cut edge. Zirconium, fluoride or copper detection in the EDS analysis indicates the presence of the silane pretreatment layer.

Figure 4.23 shows the corrosion spreading from the scribe after the paint has been removed on a panel with the silane based pretreatment, material F. The shape of the blisters are more distinct and round shaped than on the panels from the lab exposure with the same pretreatment (Fig. 4.15). No secondary blisters are seen. No growth rings are observed. The scribe is homogenous in similarity with the field exposed phosphated panel.

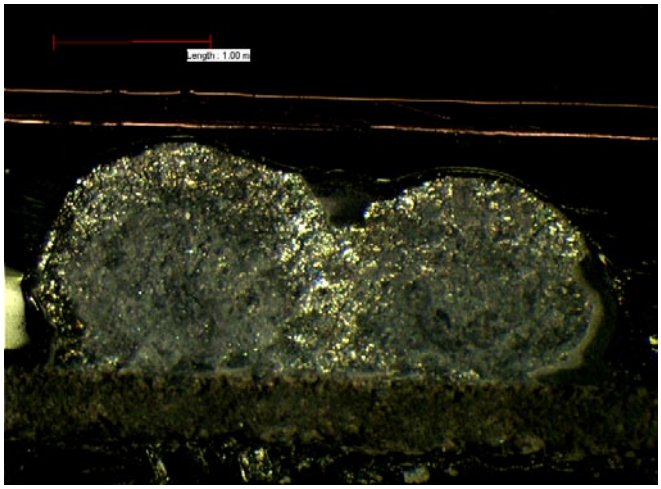

Figure 4.23. *Corrosion spreading from scribe on material F.*

In figure 4.23 the paint has been removed. The flake was analyzed and the result from EDS analysis is presented in table 4.19. The analysis was performed in low vacuum mode in an attempt to detect zirconium. The corrosion products are highly chlorine containing in accordance with the result from the lab exposed panels. The corrected values (corr Zn and corr O) in table 4.19 are calculated in the same manner as described in chapter 4.1.1. The corrosion product is a zinc hydroxy chloride. The ratio Zn/Cl is reasonably near 2,5 which is the same ratio as for simonkolleite.

Table 4.19. *Atomic composition from backside of paint material F, 20kV.*

| S | C | O | Al | Si | Cl | Ti | Zn | Zr | Corr Zn | Corr O | Zn/Cl | O/Zn | C/Zn |
|---|---|---|---|---|---|---|---|---|---|---|---|---|---|
| 0,4 | 23,24 | 37,79 | 0,54 | 0,82 | 8,62 | 1,24 | 27,04 | 0,31 | 25,81 | 30,2 | 2,99 | 1,17 | 0,90 |

Table 4.19 also shows significant amounts of zirconium on the backside of the paint on material F. No zirconium was found on the substrate side. Therefore the pretreatment layer seems to be attached on the backside of the paint in conformity with the result from the lab exposed panels (panels with silane- and zirconium based pretreatment).

Figure 4.24 shows the corrosion spreading from the edge after the paint has been removed on a panel with the silane based pretreatment, material F. As the picture shows, the corrosion seems to have spread out along the edge. This is different from the corrosion spreading from the scribe. The corrosion spread from the scribe is visible shaped more spherical than in figure 4.24. No secondary blisters and no growth rings are observed.

Figure 4.24. *Corrosion spreading from edge on material F.*

#### 4.2.2.1 Conclusions Regarding Panels with Silane Based Pretreatment from Field Exposure

The corrosion product found is a zinc hydroxy chloride, mainly simonkolleite, in well accordance with the result from the lab exposed panels. The pretreatment layer seems to be attached on the backside of the paint also in conformity with the lab exposed panels (panels with silane- and zirconium based pretreatments).

The appearance of the blister is different between the corrosion spread from scribe and edge. The corrosion spread from scribe is spherical and more distinct compared to the edge corrosion which seems to spread along the edge in an elongated manner.

The appearance of the blister from the field exposed panel is different compared to the lab exposed panel with the same pretreatment. The blister is more topographic and round shaped on the field exposed panel, which could indicate different corrosion mechanisms between the two exposure methods.

### 4.2.3 Zirconium Based Pretreatment

The result from analysis of the panel with zirconium based pretreatment, material G, from field exposure are presented in this chapter. The panel is evaluated both from scribe and from the cut edge. Zirconium present in EDS analyze indicates pretreatment.

Table 4.20 shows the result from EDS analysis for the panel with zirconium based pretreatment, material G. The table shows results from backside of the paint and from the substrate side. The analysis was performed in low vacuum mode. The corrosion products were highly chlorine containing in conformity with the result from the lab exposure presented in chapter 4.2.2. The result is also in good agreement with the lab exposed panels. The corrected values are calculated as previous described in chapter 4.1.1. The Zn/Cl ratio indicates a zinc hydroxy chloride.

Table 4.20. *Atomic composition from corrosion from scribe material G, 20kV.*

| | Ti | C | O | Al | Si | Cl | Fe | Zn | Zr | Corr Zn | Corr O | Zn/Cl | O/Zn | C/Zn |
|---|---|---|---|---|---|---|---|---|---|---|---|---|---|---|
| Backside of paint | 1.97 | 24,94 | 45,25 | 0,79 | 1,09 | 6,94 | 0,11 | 18,19 | 0.62 | 16,56 | 37,36 | 2,39 | 2,26 | 1,51 |
| Substrate | | 33,64 | 30,48 | 0,18 | 0,19 | 7,69 | 0,64 | 27,14 | | 26,86 | 28,11 | 3,49 | 1,05 | 1,25 |

Table 4.20 also shows that there is considerable amounts zirconium present on the backside of the paint. No zirconium is present on the substrate side. In accordance with previous results it is proposed that the pretreatment layer is attached to the backside of the paint.

Figure 4.25 shows the corrosion spread from the edge on a panel with the zirconium based pretreatment, material G. The left picture shows the appearance of the blister with the paint still in place. The paint has been removed in the right picture in figure 4.25. The appearance of the corrosion spread from the edge is similar to figure 4.23 (the panel with silane based pretreatment). No growth rings are seen and no signs of secondary blister formation are observed.

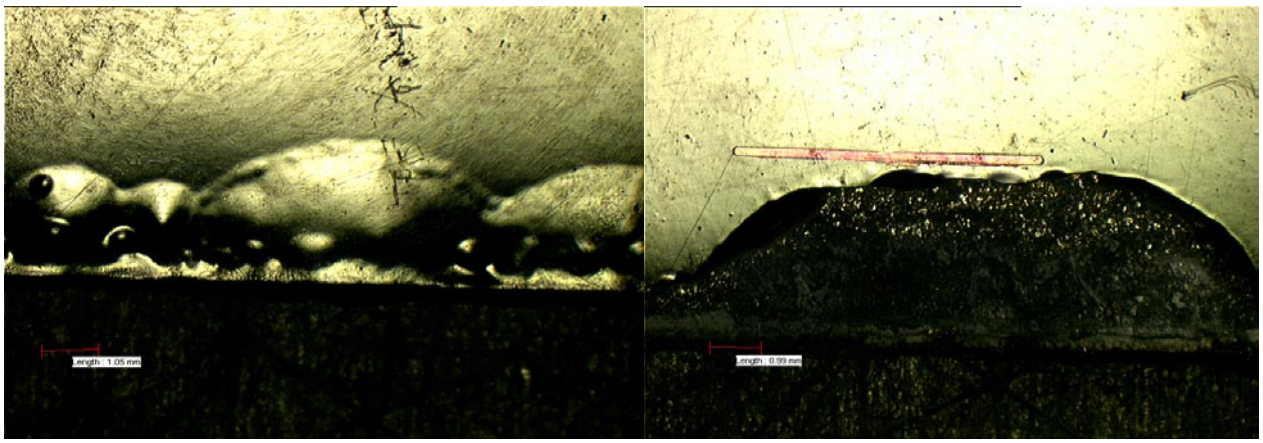

Figure 4.25. *Corrosion spreading from edge on material G.*

Table 4.21 presents the result from the EDS analysis from the edge on material G (panel with the zirconium based pretreatment). The table includes results from both backsides of the paint and the substrate. The analysis was performed in low vacuum mode. The Zn/Cl ratio is calculated to a value reasonably close to 2,5. The suggested corrosion product is therefore simonkolleite in accordance with the result presented in this study.

Table 4.21. *Atomic composition from corrosion from edge material G, 20kV.*

| | Ti | C | O | Al | Si | Cl | Fe | Zn | Zr | Corr Zn | Corr O | Zn/Cl | O/Zn | C/Zn |
|---|---|---|---|---|---|---|---|---|---|---|---|---|---|---|
| Backside of paint | 3.49 | 16,93 | 49,62 | 0,68 | 1,15 | 7,61 | 0,14 | 19,57 | 0.68 | 17,85 | 41,49 | 2,34 | 2,33 | 0,95 |
| Substrate | | 9,04 | 49,5 | 0,21 | | 10,97 | 0,18 | 29,88 | | 29,88 | 48,92 | 2,72 | 1,64 | 0,30 |

Table 4.21 shows zirconium on the backside of the paint in conformity with the lab exposed panels (panels with silane- and zirconium based pretreatments). No zirconium was found on the substrate side.

#### 4.2.3.1 Conclusions Regarding Panels with Zirconium Based Pretreatment from Field Exposure

The corrosion product found on the panel with zirconium based pretreatment is a zinc hydroxy chloride, mainly simonkolleite. The pretreatment layer seems to be attached to the backside of paint. These results are in well accordance with the result previously presented in chapter 4.

The appearance of the corrosion spread from the edge is similar to the one observed on the panel with silane based pretreatment. No growth rings were observed.

# 5 Discussion

This chapter will interpret the results presented in chapter 4. Suggestions to possible mechanisms will be argued and described.

## 5.1 Corrosion Products Formation

### 5.1.1 Statements

The study shows that simonkolleite (or a closely related zinc hydroxy chloride) was formed in the corrosion spreading from the scribe underneath the coating. No other corrosion product was found there. The corrosion spread from scribe is in the form of concentric half rings on the ACT II exposed panels with its centre in a point of the scribe (Fig. 4.18). In that centre point of the scribe zinc oxide (ZnO) has been detected (Ch. 4.1.1.1 and 4.1.2.1). This point turned lilac with phenolphthalein indicator showing the presence of a high pH. A typical growth ring pattern is seen on the panels from cyclic exposure (Fig. 5.1). On the field exposed panels the growth ring pattern is not seen.

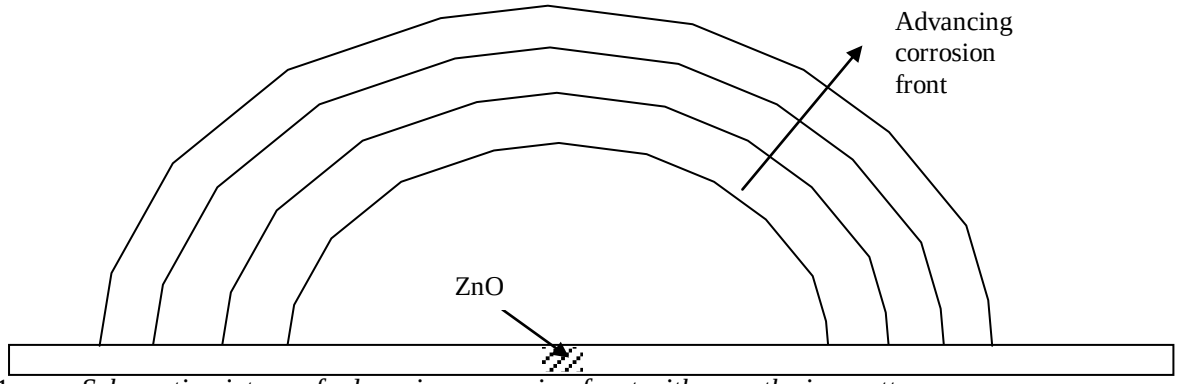


Figure 5.1. *Schematic picture of advancing corrosion front with growth ring pattern.*

The shape of the corrosion spread on the phosphated panel from cyclic exposure is spherical with secondary blisters. On the NGPT´s panels the shape of the corrosion blister is less topographical compared to the phosphated panel and no secondary blisters are seen. The shape of the blisters on the field exposed panels is different compared to the lab exposure. This is the case for both the phosphated panel and the silane based pretreated panel. This indicates that the two different exposure methods give rise to different corrosion mechanisms. No secondary blister formation is seen on the NGPT´s; however tendencies to secondary blister formation are seen on the phosphated panel from field exposure. The corrosion spread from the edge on the field exposed panels is not spherical. Instead it looks like the corrosion has spread along the edge and has not originated from a specific spot.

### 5.1.2 Previous Studies

Previous studies have been made studying corrosion under a glue layer [27]. The same blister formation was seen and the same corrosion products were detected as in this study. There were thus reasons to believe that the mechanisms for the case of corrosion under glue layers and corrosion under coating would be the same. The study showed a cathodic front moving after the anodic front (Fig.5.2); however this is not the case in this study. Several observations in this study oppose that theory; no signs of cathodic activity under the blister could be found neither from pH-indicator analysis nor from the potassium ion gradient.

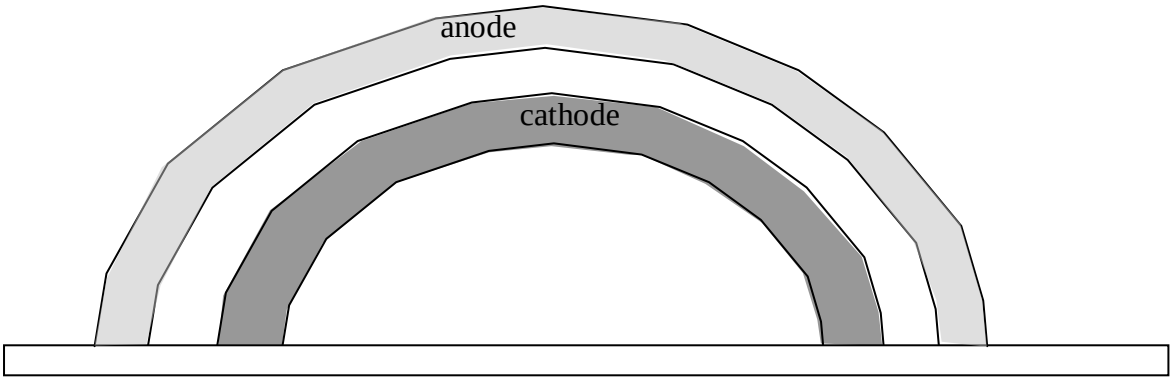


Figure 5.2. *Animated picture of a corrosion blister where the cathodic front is moving after the anodic front.*

### 5.1.3 Interpretations

The observations described in chapter 5.1.1 will be interpreted in this chapter.

The corrosion occurs due to separation of the cathode and the anode. The cathode is present in a point in the scribe and the anode is the spreading of corrosion under the coating forming zinc hydroxy chloride (possibly simonkolleite). The cathodic and anodic reactions are presented in equation 5.1 and 5.2 (Fig. 5.3). The hydroxide formation in equation 5.1 give rise to the high pH indicated by phenolphthalein.

*Cathodic reaction, oxygen reduction:*

$$\tfrac{1}{2}O_2 + H_2O + 2e^- \rightarrow 2OH^- \qquad (5.1)$$

*Anodic dissolution of zinc:*

$$Zn(s) \rightarrow Zn^{2+} + 2e^- \qquad (5.2)$$

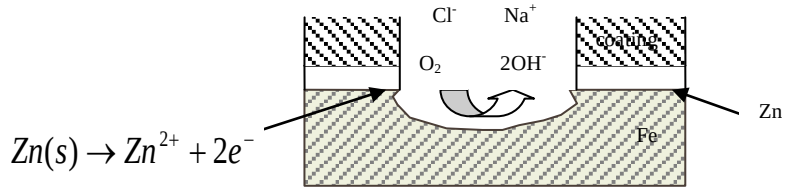


Figure 5.3. *Schematic picture over the initial stage in the scribe.*

The formation of ZnO in the scribe can be explained by the following mechanism. The cathodic area will have a high pH, due to hydroxide ion formation. As mentioned in chapter 2.5.1 cations like $Zn^{2+}$ present in electrolyte will be attracted to the cathode. The following reactions will take place in the scribe:

$$Zn^{2+} + 2OH^- \rightarrow Zn(OH)_2(s) \qquad (5.3)$$

$$Zn(OH)_2(s) \leftrightarrow ZnO(s) + H_2O \qquad (5.4)$$

The reaction from zinc hydroxide to zinc oxide happens fast. For instance, during the drying cycles, the equilibrium 5.4 would most certainly be pushed to the right side. Furthermore, zinc oxide is an n-type semiconductor (in contrast to zinc hydroxide which is an insulator) and will therefore significantly accelerate the cathodic reaction.

The anodic area will have a slightly acidic pH due to hydrolysis caused by dissolving zinc ions. Anions are pulled towards the anode because of the higher electrical potential at this site. The following consecutive reactions are possible:

$$Zn^{2+} + 2Cl^- \rightarrow ZnCl_2(aq) \quad (5.5)$$

$$5Zn^{2+}(aq) + H_2O + 8OH^-(aq) + 2Cl^-(aq) \rightarrow Zn_5Cl_2(OH)_8 * H_2O(s) \quad (5.6)$$

The stability diagram made by Lindström [19] shows that simonkolleite $Zn_5Cl_2(OH)_8*H_2O$ will form at a pH around 5,5-8 (Fig. 5.4) and at a high chlorine concentration. It is likely that these circumstances occur in the anodic areas during the cyclic exposure.

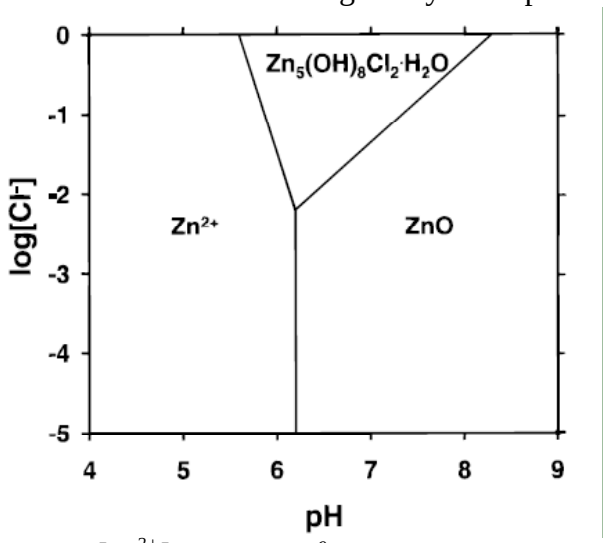


Figure 5.4. *Stability diagram, $[Zn^{2+}]$=0,1M at 25°C.*

The formation of simonkolleite by a solid state equation (Eq. 5.7) can however not be excluded:

$$5Zn + 2Cl^- + 9H_2O \rightarrow Zn_5Cl_2(OH)_8 * H_2O + 10e^- + 8H^+ \quad (5.7)$$

It is not likely that zinc chloride, $ZnCl_2$, precipitates as crystals due to a very high solubility product for that compound. A chloride concentration of ~5M is needed to form crystals, the panels have been subjected to a salt concentration of 0,1M. It is therefore more likely to believe that simonkolleite will be formed instead.

### 5.1.4 Electrical Current Calculations

To theoretically prove that it is possible for a small spot in the scribe to run an advancing anodic front; current and potential drop calculations are made.

By calculating the current it is possible to confirm the possibility for the suggested cathode to support the anodic front with enough current. Figure 5.5 shows a picture with written values used in this calculation example. The values are typical ones obtained from the corrosion after six weeks in ACT II. The average anodic current is obtained from the mass loss of metallic zinc using Faraday's law.

*Half cell reactions:*

$$Zn \rightarrow Zn^{2+} + 2e^{-} \quad (5.8)$$

$$O_2 + 2H_2O + 4e^{-} \rightarrow 4OH^{-} \quad (5.9)$$

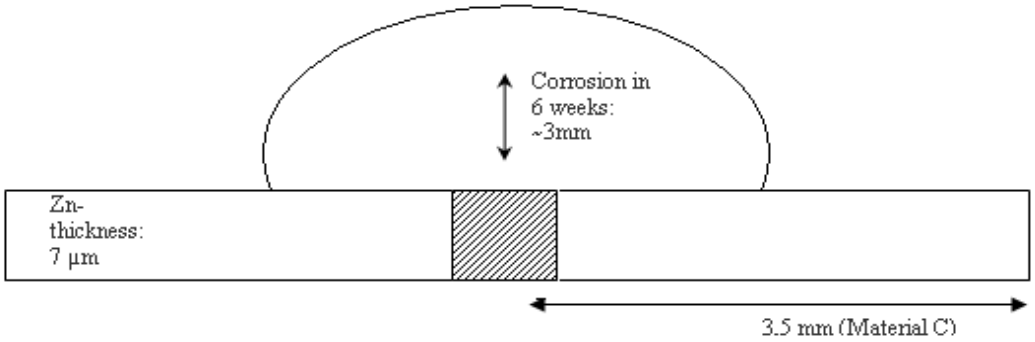


Figure 5.5. *Schematic picture of corrosion picture, data taken from material C.*

Table 5.1 *Data for zinc oxidation, constants and material parameters.*

| | |
|---|---|
| Height of corrosion cell, h | 0,3cm |
| Ratio of corrosion cell, b | 0,35cm |
| Time, t | 6 weeks = 3628800s |
| Zn- thickness, δ | 0,0007cm |
| Density, $\rho_{zinc}$ | 7,14g/cm$^3$ |
| Molar mass, $M_{zinc}$ | 65,37g/mol |
| Faraday's constant, F | 96487As/mol |
| Number electrons in the half cell reaction, $N_1$ (Eq. 5.8) | 2 |

The following calculations are based on the example when the ratio of corrosion cell is 3,5 mm. The calculated value is an average value of the anodic current flowing during the 6 weeks of exposure.

Corroded volume: $V = 0{,}35^2 * \pi * 0{,}0007/2 = 0{,}000135 cm^3$

Mass of corroded zinc: $m = 0{,}000135 * 7{,}14 = 0{,}00096 g$

Moles of corroded zinc: $n = 0{,}00096/65{,}37 = 1{,}47 * 10^{-5} mol$

Used amount of current: $I * s = 1{,}47 * 10^{-5} * 96487 * 2 = 2{,}8 As$

Average current: $I_{cell} = 2{,}8/3628800 = 7{,}81 * 10^{-6} A$

The average current for anodic oxidation is $7{,}81*10^{-6}$A.

The calculations concerning the cathodic current are based on the assumption that the oxygen reduction is localized in a small spot in the scribe and that the speed of the reduction has reached the limit current density (i.e. diffusion of oxygen through the aqueous phase to the cathode site is the rate limiting step). The width of the cathodic spot equals the scribe width, 0,5 mm. Also the breadth is estimated to be the same which seems reasonable from the cathodic spot indicated by phenolphthalein in fig. 4.12. The diffusion layer thickness is estimated to be of the same order of magnitude as the depth of the scribe, ~10 µm.
The equation for the speed of the oxygen reduction will then be:

$i_{oxygen} = i_{lim} = D_{oxygen} * C_{oxygen} * N_2 * F/\delta$

Table 5.2 *Data for oxygen reduction at 20°C.*

| | |
|---|---|
| Diffusivity in water, $D_{oxygen}$ | $2{,}00*10^{-5} cm^2/s$ |
| Solubility in water, $C_{oxygen}$ | $2{,}84*10^{-7} mol/cm^3$ |
| Diffusion layer thickness, $\delta$ | 0,001cm |
| Cathodic area, A | 0,05*,05=0,0025 cm² |
| Number of electrons in half cell reaction, $N_2$ (Eq. 5.9) | 4 |

Speed of oxygen reduction:

$$v = 2{,}00*10^{-5} * 2{,}84*10^{-7} / 0{,}001*0{,}0025 = 1{,}42*10^{-11} mol/s$$

Current of oxygen reduction: $I_{oxygen} = 1{,}42*10^{-11} * 96487 * 4 = 5{,}48*10^{-6} A$

The calculation shows, that the cathodic spot in the scribe is capable of supplying a current of $5{,}48*10^{-6}$A. This is a figure matching the average anodic current calculated above. This shows that it is theoretically possible for a small cathodic spot in the scribe to run an anodic process of the size in the example above. The current for oxygen reduction is higher than the current for anodic oxidation.

### 5.1.5 Potential Drop Between Cathode and Anode

In chapter 5.1.3 it is confirmed that the cathodic current is enough to run the corrosion blister. The driving force to run the current however must also be high enough for the corrosion to be driven by a small cathodic area in the scribe. The driving force, the equilibrium potential difference between the reduction and the oxidation, respectively, must be larger than the potential drop. This is confirmed in this chapter.

The distance to the anodic front from the centre of the corrosion cell, which is assumed to be the cathode, is 0,3 cm (Fig. 5.5).

It can be shown, that the potential drop between a singular spot (the cathode in this case) and the periphery of an advancing hemi-spherical anodic front follows the equation:

$$\Delta U = I_{oxygen} * \rho / \pi / \delta * \ln(h / r_o) \qquad (5.10)$$

NaCl 0,5 weight%; molar mass: $M_{NaCl} = 0{,}5*10/(23+35{,}5) = 0{,}085 mol/l$

Equivalent conductivity, NaCl 0,1M: $\sigma_{ekv} = 109(1/ohm)*l*mol$

Conductivity: $\chi = 109 * 0{,}085 = 9{,}32(1/ohm/cm)$

Resistivity: $\rho = 1/9{,}32 = 0{,}11(ohm*cm)$

Initial radius: $r_0 = 0{,}025cm$

Potential drop:

$$\Delta U = 5{,}48*10^{-6} * 0{,}11/3{,}14/0{,}0007 * \ln(0{,}3/0{,}025) = 7{,}42*10^{-4} V$$

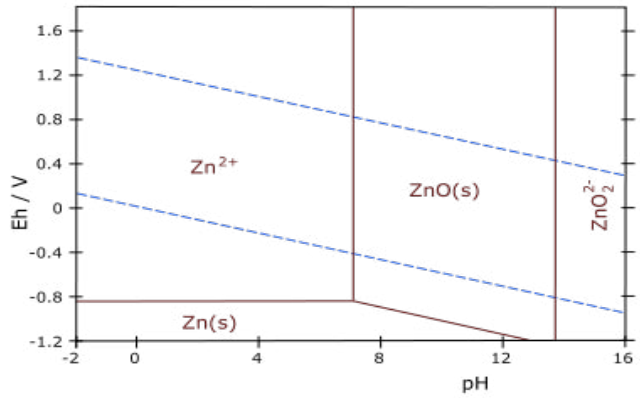


Figure 5.6. *Pourbaix diagram zinc.*[5]

The potential drop between cathode and anode is $7{,}42*10^{-4}$V. From the Pourbaix diagram (Fig. 5.6) the equilibrium potential for oxygen reduction and for zinc oxidation can be approximated. At a neutral pH the equilibrium potential for oxygen reduction is 0,9V and for zinc oxidation -0,8V. This gives a resulting equilibrium potential difference of 1,7V. This value can be compared with the calculated potential drop of $7{,}42*10^{-4}$V. This clearly shows that there is enough driving force to run the whole blister.

### 5.1.6 Growth Rings

The growth rings on the backside of the paint and the metal substrate are correlated to each other in the following way. A build up representing a ring on the back of paint represent a pit on the substrate and vice versa (Fig. 5.7).

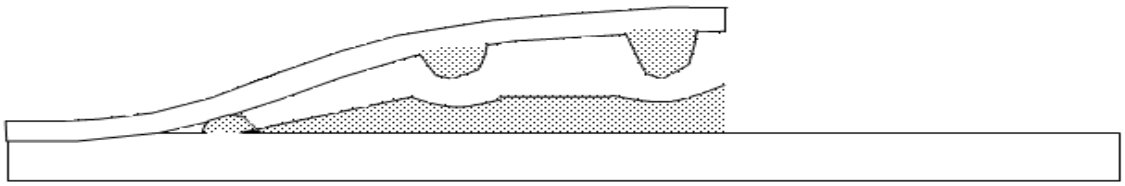

Figure 5.7. *Schematic picture of corrosion blister, where the darker area represent corrosion products.*

The number of growth rings seen in fig. 4.15 is approximately 20. The number of drying cycles in ACT II is 30. An initiation period must be taken in consideration and it is therefore suggested that the growth rings correspond with the drying cycles in ACT II.

Chapter 4.1 mentions the different morphologies and sizes of zinc hydroxy chloride. A possible explanation for this could be a relation to the cycles and to the solubility. For instance small crystals seen in the growth ring (Fig. 5.8) precipitate from a highly oversaturated liquid, which occurs in the dry periods of the ACT II cycles.

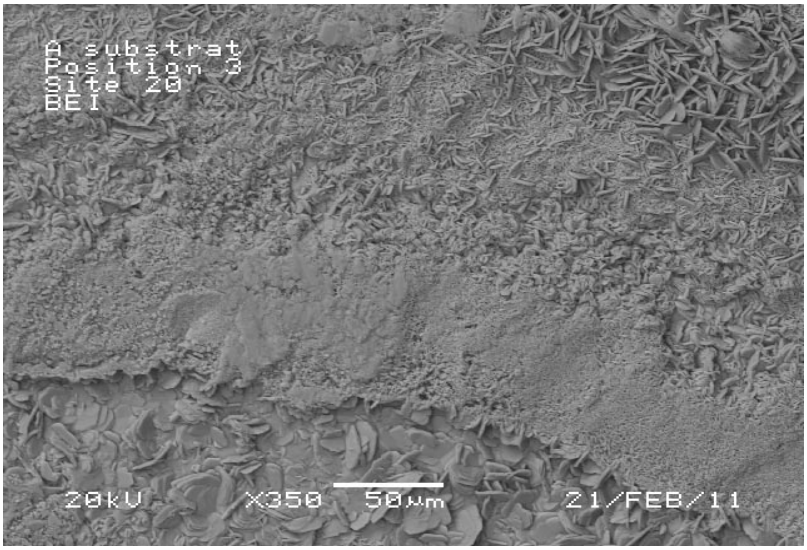


Figure 5.8. *Different simonkolleite morphologies, material A.*

The field exposed panels (material E-G) do not show any growth rings and have a featureless scribe (Fig. 5.9). The only corrosion product found in the corrosion spread from the scribe is zinc hydroxy chloride, mainly simonkolleite. Therefore the mechanism with a moving anodic front under the coating happens in the case of field exposed panels also.

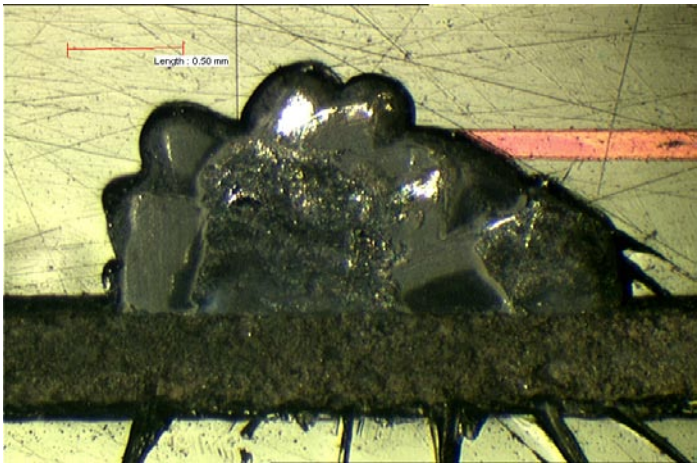


Figure 5.9. *Corrosion spreading on material E. The scribe is more homogenous than the lab exposed panel and is located in the bottom of the picture.*

Table 4.18 shows the formation of non chlorine containing corrosion products in the corrosion spread from the edge on material E. A potential explanation for this can be the more open column offered by the cut edge. This will increase the carbon dioxide concentration and decrease the chloride concentration and therefore the suggested hydrozincite is formed instead of simonkolleite. More studies need to be done in order to confirm this.

The appearance of the corrosion spread from the edge is different compared to the corrosion spread from scribe; as pictured in figure 4.25 compared to fig 5.9. The corrosion spread from the edge does not show the same distinct blisters. Instead the corrosion seems to spread along the edge. Therefore the mechanism is suggested to be different in this case. Other corrosion

products are also found as mentioned in the section above. More investigations need to be made in this area.

## 5.2 Advancement of Corrosion Front and the Influence of the Pretreatment Layer

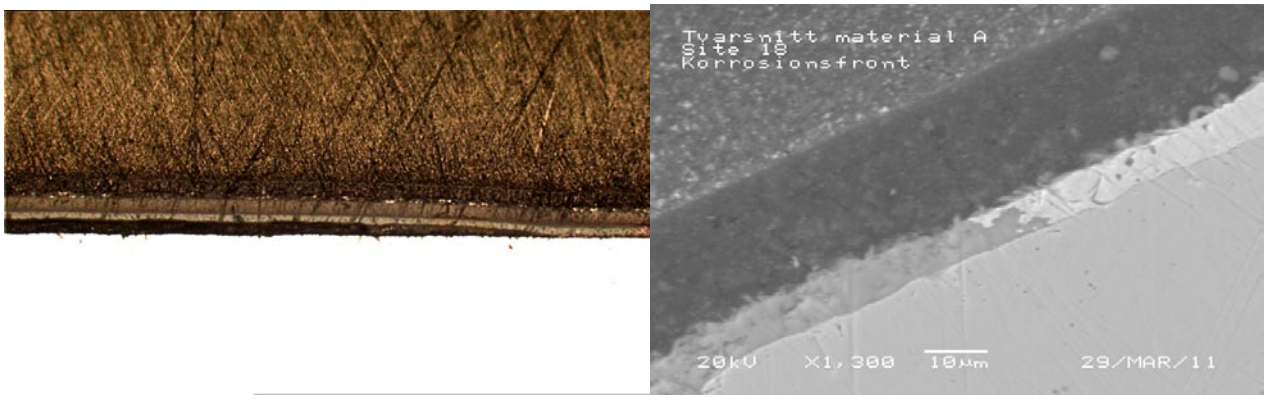


Figure 5.10. *Corrosion front in cross section of material A, stereo microscope (left) and SEM (right).*

The expansion of corrosion products tends to open the metal/paint interface as seen in figure 5.10. Zinc hydroxy chloride is formed according to figure 5.11 and equation 5.6 and takes up more space than the original zinc layer. This give rise to a wedge formation at the corrosion front.

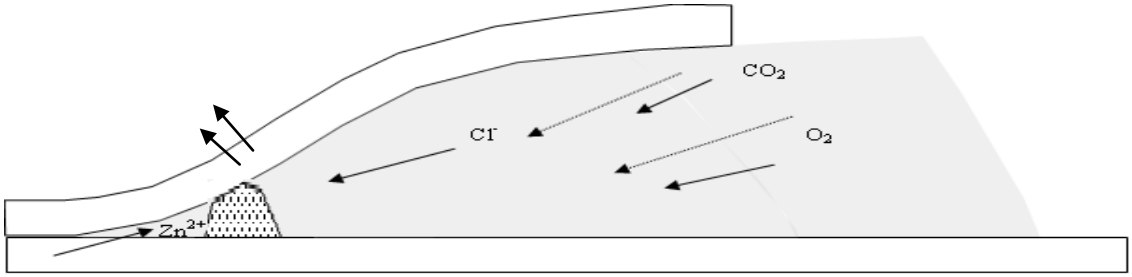


Figure 5.11. *Initial formation of corrosion products at the front of corrosion blister.*

### 5.2.1 Suggestions

The wedge results in a force at the corrosion front which tends to open the corrosion crack. The crack will take the easiest path, meaning that the opening occurs at the weakest interface. The crack is filled with corrosion products, in this study mainly simonkolleite. The example pictured in figure 5.12 shows that the crack occurs between the zinc and the steel layer. Hence, in this case, this is the weakest interface, weaker than the zinc/phosphate and phosphate/paint interfaces.

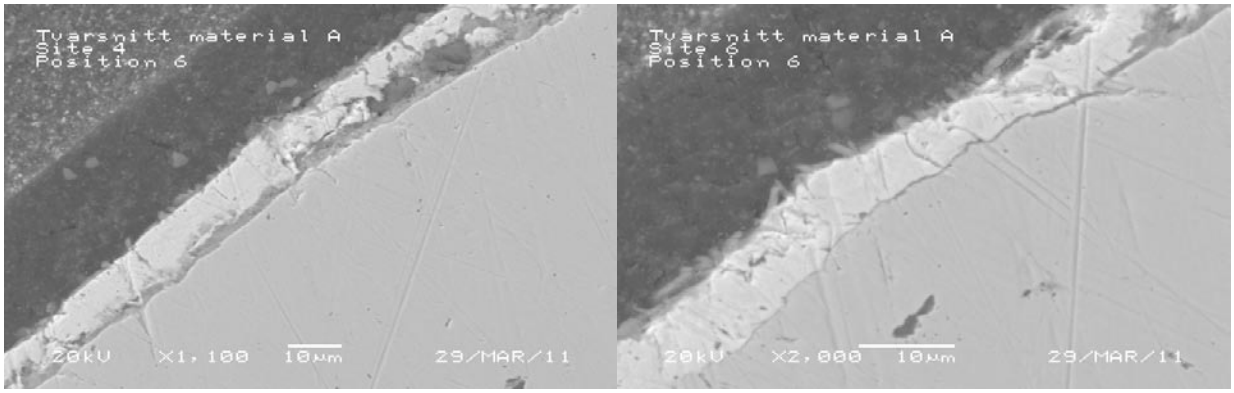


Figure 5.12. *Crack formation between zinc and steel interface. The left picture showing the corrosion front and the initial formation of crack and the right picture show the continued crack.*

Normally, however, on phosphated samples, the delamination occurs between the phosphate layer (which is left on the paint side of the crack) and the zinc layer. An example of this is the unaffected phosphate layer confirmed in chapter 4.1.1 and pictured in figure 4.11. The intact phosphate layer present on the backside of the paint shows that the opening is between zinc and phosphate layer. This further confirms a strong bonding between ED coating and pretreatment. On the field exposed panel from scribe however significant amounts phosphorous were found on both backside of paint and substrate. This indicates that a different mechanism is active in the field exposure compared to the ACT II exposure.

For the silane based and zirconium based pretreatment, zirconium was found on the backside of the paint only (Ch. 4.1.2-4.1.3). This once again shows that the weakest interface is between the zinc and the pretreatment layer. This is also the case for all the the field exposed panels.

# 6 Conclusions

In this study several analyses concerning corrosion under paint coating have been made in an attempt to understand the corrosion mechanism. Analyses regarding different pretreatments have also been preformed. The samples have been subjected to cyclic testing (ACT II) and field exposure.

In this study the most existent corrosion product is a simonkolleite or a closely related zinc hydroxy chloride. Simonkolleite is found on all materials despite different exposure methods and pretreatments. SEM analysis shows different structures and crystal sizes of the zinc hydroxy chloride but EDS analysis show the same elemental composition.

The shape of the corrosion spread on the phosphated panel from cyclic exposure is spherical with secondary blisters. On the NGPT´s panels the shape of the corrosion blister is less topographical compared to the phosphated panel and no secondary blisters are seen. The shape of the blisters on the field exposed panels is different compared to the lab exposure. This is the case for both the phosphated panel and the silane based pretreated panel. This indicates that the two different exposure methods give rise to different corrosion mechanisms. No secondary blister formation is seen on the NGPT´s; however tendencies to secondary blister formation are seen on the phosphated panels.

The cathode is separated from the anode on the ACT II exposed panels. The cathode is found in a small spot in the scribe according to results in this study from cyclic exposure. Several observations prove this statement. The small spot runs the whole corrosion spread under the paint which acts as an anode. On the panels from the cyclic exposure the spreading is semicircular. On the field exposed panels the scribe is homogenous compared to the rougher scribe from the lab exposure. The cathode in this case is not a specific spot but instead a more diffuse area. The corrosion spread from the edge on the field exposed panels is not spherical. Instead it looks like the corrosion has spread along the edge and is not originated from a specific spot.

Growth rings are observed on the panels from the cyclic exposure. The growth rings are differently distinct depending on pretreatment. On the phosphated panel only tendencies to growth ring formation is seen. On the silane based pretreated panel the growth rings are easier to distinguish and on the zirconium based panel the growth rings are very distinct. These growth rings are buildups of corrosion products, zinc hydroxy chloride (simonkolleite). The growth rings seem to be related to the cycles in the global laboratory accelerated cyclic corrosion tests. Growth rings are not found on panels from field exposure.

The mechanism behind the coating disbondment starts with a wedge formation lifting the coating from substrate with a mechanical effect. The wedge is a buildup of zinc hydroxy chloride (simonkolleite) formed at the front of the corrosion blister.

The pretreatment is crucial for the corrosion mechanism. The different pretreatments evaluated in this study show differences and similarities in corrosion behavior. The corrosion product is the same despite different pretreatments used and the mechanism tends to be same for the lab exposed panels. The adhesiveness of the paint coating is highly dependent on the pretreatment.

Analyses show an intact pretreatment layer present on the backside of the paint from the cyclic exposure. This observation indicates good bonding between the pretreatment and paint coating. Bending test performed to evaluate the adhesion of different pretreatments generally showed that fracture occurred within the pretreatment layer for all three types of pretreatments. This confirms good bonding between the pretreatment and the paint coating.

# 7 Future Work

Simonkolleite was detected as the main existent corrosion product with help of SEM/EDS analysis and to some extent FTIR. In an attempt to see if other corrosion products may be present other analysis methods would be useful. X-ray diffraction and microscope-FTIR are suitable for this purpose.

The study focused on analyzing HDG panels. The same work should be done on other materials, e.g. cold-rolled steel, to see which corrosion products are formed, investigate mechanisms and to see if the pretreatment behaves differently.

In order to confirm and understand the relation to the cycling in corrosion test chambers a more complete study should be made in this area. In situ studies on the corrosion blisters would be able to give information regarding initiation of blister and the kinetics. The kinetic could possible give a relation between corrosion spread as a function of time. The study suggests precipitation of corrosion products during a dry period in the corrosion chamber,

which would result in a growth ring buildup at every dry period. If the time in the corrosion is doubled then this would mean that the amount of growth rings should also be doubled. More research must be made.

The cathodic area is localized in the scribe, but the initiation of this area is not known. How is this specific cathode formed? More studies in this area should be made by studying the initial formation of the corrosion blister. The differences in scribe appearance from different exposure methods should also be studied. The corrosion from edge is different from the corrosion from the scribe. Why is this different?

To see differences in blister formation due to different pretreatments, the angle in the corrosion blister front between substrate and coating could be measured. Is the angle bigger or smaller for different pretreatments and how does this affect the corrosion mechanism?

Further studies on field panels should be made. The mechanism from the cut edge seems to differ from corrosion from scribe and the reason for this is unknown.

# 8 References


1. Jones D.A. (1996): *Principles and Prevention of Corrosion.* Prentice Hall, Upper Saddle River, New Jersey, USA.
2. VCC standard: CETP 000-L-467; *Global Laboratory Accelerated Cyclic Corrosion Test*
3. Amirudin A., Thierry D. (1996): Corrosion mechanisms of phosphated zinc layers on steel as substrates for automotive coatings. *Progress in Organic Coatings*, No. 28, pp. 59-76.
4. Svensson G. (2005-2006): *Blister Corrosion- development of present test method and analysis of corrosion products,* Master Thesis, Department of Environmental Inorganic Chemistry, Chalmers University of Technology, Göteborg, Sweden.
5. Philipe A., Schweitzer P.E. (2003): *Metallic Materials: Physical, Mechanical, and Corrosion Properties.* Marcel Dekker, New York, USA.
6. Ogle K., Tomandl A., Meddahi N., Wolpers M. (2004): The alkaline stability of phosphate coatings I: ICP atomic emission sepctroelectrochemistry. *Corrosion Science*, No. 46, pp.979-995.
7. Educational day VCC: *Surface Treatment*. 2011-04-14
8. Lindqvist K., Persson D., Öhman M., Österberg L. (2010): *Characterisation of commercial novel surface pre treatments on aluminium, HDG steel and carbon steel and comparative environmental studies*. Swerea.
9. Tegehall, P-E. *The Chemistry of Zinc Phosphating of Steel*, Doctoral Thesis, Department of Inorganic Chemistry, Chalmers University of Technology, Göteborg, Sweden.
10. Sabata A. (1989): *Study of the corrosion mechanisms in modern painted precoated automotive sheet steels*, Doctoral Thesis, Department of Material Science. Colorado School of Mines, Colorado, USA.
11. Kuhm P., Huys P. *Tectalis, the successor to zinc phosphate learning experience after running 1 year at different car body lines.* Henkel AG & Co, Dusseldorf, Germany.
12. Adhikari S., Unocic K.A., Zhai Y., Frankel G.S., Zimmerman J., Fristad W. (2011): Hexafluorozirconic acid based surface pretreatments: Characterization and performance assessment. *Electrochimica Acta*, No. 56, pp. 1912-1924.
13. Lunder O., Simensen C., Yu Y., Nisancioglu K. (2004): Formation and characterisation of Ti-Zr based conversion layers on AA6060 aluminium. *Surface and Coatings Technology*, No. 184, pp. 278-290.
14. Schmidt-Hansberg Th., Schubach P. (2001): A comparative study of innovative aluminium pretreatments. *Galvanotechnik,* Vol. 92, No. 12, pp. 9-14.
15. Chico B., et Al. (2007): Elecrochemical impedance spectroscopy study on the effect of curing time on the early barrier properties of silane systams applied on steel substrates. *Process in Organic Coatings*. Vol. 60, pp. 45-53.
16. Nockert J. *Interaction between paint under-cutting and the mechanical properties of the coating,* Master Thesis, Department of Corrosion Science, Royal Insitute of Technology, Stockholm, Sweden. (2006)
17. Marcus P. (2002): *Corrosion Mechanisms in Theory and Practice*. Macel Dekker, New York, USA.
18. Odnevall, I. *Atmospheric Corrosion of Field Exposed Zinc- a multianalytical characterisation of corrosion products from initial films to fully developed layers.* Doctoral Thesis, Royal Institute of Technology, Stockholm, Sweden (1994)
19. Lindström R., Svensson J-E., Johansson L-G. (2000): The Atomospheric Corrosion of Zinc in the Prescence of NaCl- The Influence of Carbon Dioxide and Temperature. *Journal of the Electrochemical society*. Vol. 147, No. 5, pp. 1751-1757.

20.Graedel T.E. (1989): Corrosion Mechanisms for Zinc Exposed to the Atmospere. *Journal of the Electrochemical society*. Vol. 136, No. 4, pp. 193-203.
21. Bautista A. (1996): Filiform corrosion in polymer-coated metals. *Progress in Organic Coatings*, No. 28, pp. 49-58.
22. VCC standard: VCS 1021,29; *Scribing of coated test object and evaluation of propagation of corrosion from scribed line*
23. VCC standard: VCS 1024,2529- *Bending Test*
24. *Invitation to the SEM world*, handbook, JEOL Ltd.
25.A guide to scanning microscope observation, application note, JEOL Ltd.
26. Cademartiri L., Ozin A. G. (2009): *Concepts of Nanochemistry*. Wiley-VCH Verlag GmbH, Weinheim, Germany.
27. LeBozec N., Persson D., Thierry D. (2004): In Situ studies of the initiation of propagation of filiform corrosion of aluminium. *Journal of the Electrochemical society*. Vol.151, No. 7, pp. B440-B445.

## Appendix I- Corrosion Products

Table A.1 *Minerals containing zinc and other crystalline substance with possible relevance to the corrosion of zinc.*

| Substance | Crystal System | Formula |
|---|---|---|
| ***Metal, oxides and hydroxides*** | | |
| Zincite | Hexagonal | ZnO |
| Zinc hydroxide | Tetragonal | $Zn(OH)_2$ |
| ***Sulfides*** | | |
| Würtsite | Hexagonal | β-ZnS |
| ***Sulfites*** | | |
| Zinc sulfites | Monoclinic | $ZnSO_3*2H_2O$ |
| ***Sulfates*** | | |
| Zinkosite | Orthohombic | $ZnSO_4$ |
| Gunningite | Monoclinic | $ZnSO_4*H_2O$ |
| Bianchite | Monoclinic | $ZnSO_4*6H_2O$ |
| Goslarite | | $ZnSO_4*7H_2O$ |
| Zinc sulfate | - | $Zn_4SO_4(OH)_6$ |
| Zinc sulfate | - | $Zn_7SO_4(OH)_{12}*4H_2O$ |
| ***Chlorides*** | | |
| Simonkolleite | Hexagonal | $Zn_5Cl_2(OH)_8*H_2O$ |
| Zinc oxychloride | - | $Zn_5Cl_2O_4*H_2O$ |
| ***Carbonates*** | | |
| Smithsonite | Trig. | $ZnCO_3$ |
| Zinc carbonate | - | $ZnCO_4* H_2O$ |
| Zinc carbonate | - | $Zn_4CO_3(OH)_6$ |
| Hydrozincite | Monoclinic | $Zn_5(CO3)_2(OH)_6$ |
| ***Nitrates*** | | |
| Zinc nitrate | - | $Zn(NO_3)_2$ |

## Appendix II- Scribing

The figures are showing the scribing technique and template according to *VCS 1021,29.*

Figure A.2 *Applying the scribed line.*

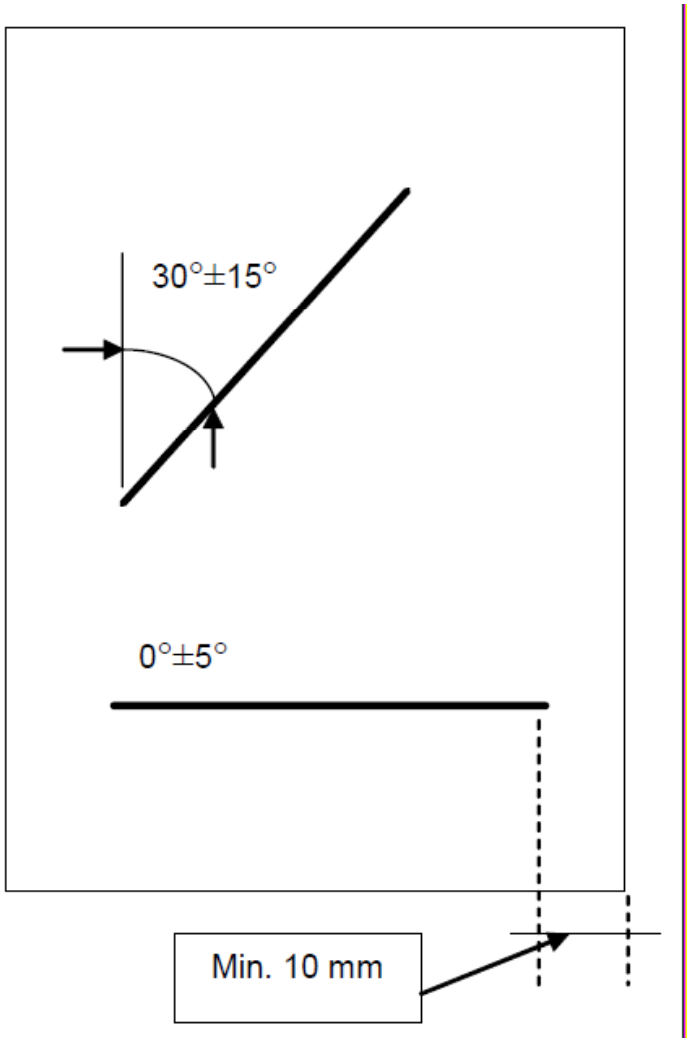


Figure A.3 *Scribing on test panel, template.*

# Appendix III- Global Laboratory Accelerated Cyclic Corrosion Test

Table A.1 *Climate program, step by step in automated mode.*

| Step | Time elapsed | | Duration of step | | Climate settings at start of step | | Comments |
|---|---|---|---|---|---|---|---|
| no | h | m | h | m | T (°C) | % RH | |
| 1a | 0 | 0 | 0 | 10* | 50* | 70* | Spray thoroughly 0.5% NaCl to wet and cool |
| 1b | 0 | 10 | 0 | 20 | 30-50 | wet | Cool chamber with maximum capacity |
| 1a' | 0 | 30 | 0 | 3 | <30 | wet | Spray to regain wetness (cooling dries) |
| 1c | 0 | 33 | 2 | 27 | <30 | wet (95) | 25±2 to be reached within 1 h from start (1a) |
| 1a' | 3 | 0 | 0 | 3 | 25±2 | wet | Secure and support wetness by spraying |
| 1c' | 3 | 3 | 2 | 54 | 25±2 | wet (95) | wet (95) = OK to set to 95% RH |
| 1a' | 5 | 57 | 0 | 3 | 25±2 | wet | Defines wet condition before climate control |
| 2a | 6 | 0 | 0 | 30 | 25±2 | wet (95) | Start of quick temperature rise without drying |
| 2b | 6 | 30 | 2 | 00 | 40±0.6 | wet (95) | Start of slow drying by diffusion |
| 3a | 8 | 30 | 15 | 30 | 50±0.6 | 70±3 | Panels shall be free from visible wetness |
| 3a | 24 | 00 | - | - | 50±0.6 | 70±3 | End of "workday" procedure |
| Repeat steps 1a - 3a another four times | | | | | | | |
| 3b | 120 | 00 | 48 | 00 | 50±0.6 | 70±3 | Phase in with weekends in case of manual operations in "workday" procedure |
| 3b | 168 | 00 | - | - | 50±0.6 | 70±3 | |
| Repeat steps 1a-3b for required number of weeks | | | | | | | |

* Provided proceeding from step 3a or 3b

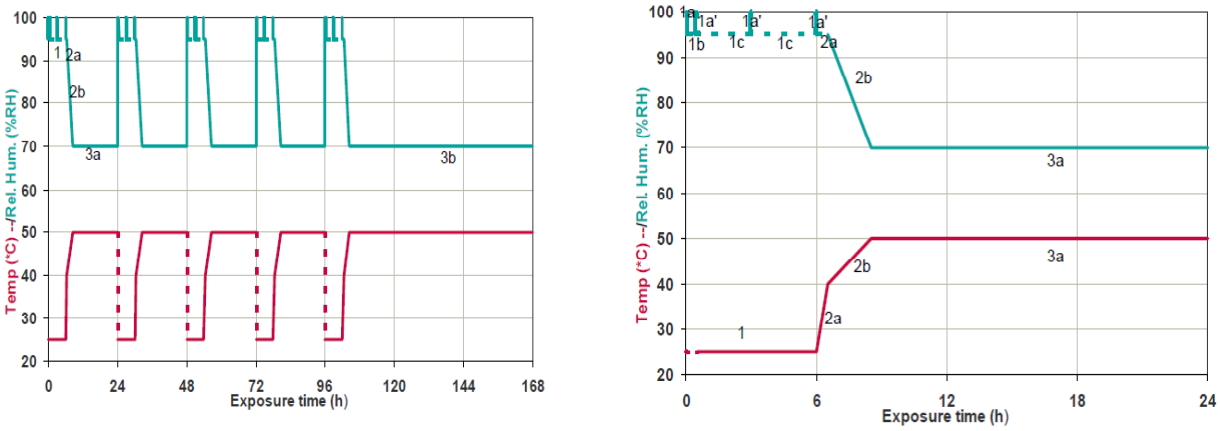


Figure A.4 *Workday (mon-fri) test cycle (left) and complete weekly program (right).*

## Appendix IV- FTIR Reference

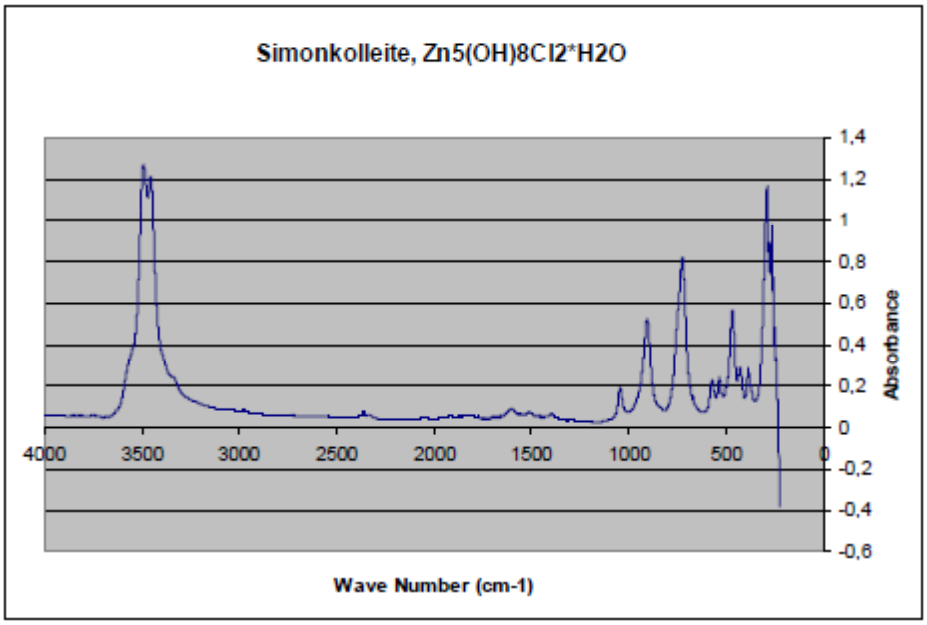


Figure A.5 *FTIR- reference simonkolleite.*